Positive and negative drag, dynamic phases, and commensurability in coupled one-dimensional channels of particles with Yukawa interactions

C. Reichhardt, C. Bairnsfather, and C. J. Olson Reichhardt

Phys. Rev. E **83**, 061404 — Published 13 June 2011

DOI: 10.1103/PhysRevE.83.061404

Positive and Negative Drag, Dynamic Phases, and Commensurability in Coupled One-Dimensional Channels of Particles with Yukawa Interactions

C. Reichhardt[1], C. Bairnsfather[1,2], and C. J. Olson Reichhardt[1]
[1] *Theoretical Division, Los Alamos National Laboratory, Los Alamos, New Mexico 87545, USA*
[2] *Department of Physics, Purdue University, West Lafayette, Indiana 47907, USA*

We introduce a simple model consisting of two or three coupled one-dimensional channels of particles with Yukawa interactions. For the two channel system, when an external drive is applied only to the top or primary channel, we find a transition from locked flow where particles in both channels move together to decoupled flow where the particles in the secondary or undriven channel move at a slower velocity than the particles in the primary or driven channel. Pronounced commensurability effects in the decoupling transition occur when the ratio of the number of particles in the top and bottom channels is varied, and the coupling of the two channels is enhanced when this ratio is an integer or a rational fraction. Near the commensurate fillings, we find additional features in the velocity-force curves caused by the slipping of individual vacancies or incommensurations in the secondary channels. For three coupled channels, when only the top channel is driven we find a remarkably rich variety of distinct dynamic phases, including multiple decoupling and recoupling transitions. These transitions produce pronounced signatures in the velocity response of each channel. We also find regimes where a negative drag effect can be induced in one of the non-driven channels. The particles in this channel move in the opposite direction from the particles in the driven channel due to the mixing of the two different periodic frequencies produced by the discrete motion of the particles in the two other channels. In the two channel system, we also demonstrate a ratchet effect for the particles in the secondary channel when an asymmetric drive is applied to the primary channel. This ratchet effect is similar to that observed in superconducting vortex systems when there is a coupling between two different species of vortices.

PACS numbers: 82.70.Dd,05.60.Cd

I. INTRODUCTION

There are many systems composed of repulsively interacting particles with one dimensional (1D) or quasi-1D motion, including colloids in narrow channels [1–10], Wigner crystal states in wires [11–19] and constrictions [20], dusty plasmas in grooves [21], macroscopic charged ball bearings in channels [22], and vortices in type-II superconductors confined within narrow strips or channels [23–27]. In many of these systems, interesting structural transitions from 1D lines of particles to zig-zag or buckled states can occur [4, 17, 19]. There can also be higher order transitions from 2 rows to 3 rows of particles or transitions to disordered states [5, 23, 24, 27]. Under an external drive, this type of system also exhibits a variety of dynamical behavior such as ordered or disordered motion through constrictions [1, 20, 27] or dynamic commensurability effects [23, 24].

Here we propose a simple system consisting of particles in two or three coupled 1D channels. The particles in each channel interact with the other particles in the same channel as well as with particles in adjacent channels via a Yukawa potential. An external drive applied to only one channel produces drag effects on the particles in the undriven channels, causing them to move. Our system is illustrated in Fig. 1. The two channel system is similar to the transformer geometry studied for vortices in two superconducting layers where an external drive is applied to one (primary) layer and the response of the nondriven (secondary) layer is measured [28–30]. If the vortices in the two layers are fully coupled, the response of the secondary layer is exactly the same as the response of the primary layer. If the vortices are only partially coupled, the response in the secondary layer is smaller than that of the primary layer. The transformer geometry has also been studied for vortex systems with multiple layers, such as vortices in the strongly layered high-temperature superconductors [31]. Drag effects have also been predicted for two coupled 1D wires containing classical 1D Wigner crystals when only one of the wires is driven [13]. In this case the interaction between particles in neighboring wires is repulsive, unlike the attractive interaction between vortices in neighboring layers. For the coupled 1D Wigner crystals there is also a transition from a completely locked state, where the response in both wires is identical, to a partially locked state, where the response of the secondary wire is reduced. Drag effects in coupled wire experiments have been interpreted as arising from the formation of Wigner crystal states [32].

In this work we consider the effect of changing the ratio of the number of particles in each channel on the locking or coupling between the channels, with a particular focus on ratios that are integers or rational fractions. Commensuration effects [33] occur when the spacing between particles in one channel is a simple rational fraction of the spacing between particles in another channel, while incommensurations such as vacancies or interstitials appear when the two spacings are incommensurable. Commensuration effects have been studied extensively for systems in which a varied number of particles interacts with

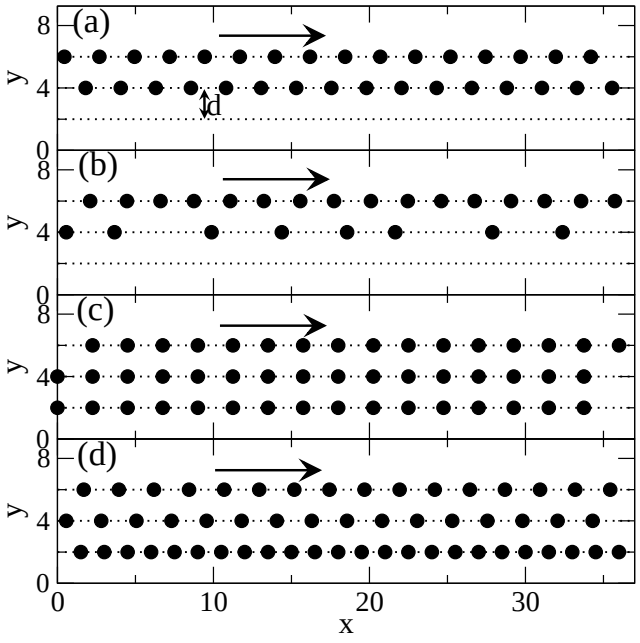

FIG. 1: Image of the sample geometry. The locations of the three channels are indicated by dotted lines. Black dots are particles within the channels. The arrow denotes the driving force which is applied only to particles within the top channel, termed the primary channel p. The bottom undriven channels are the secondary channels s_1 and s_2. The ratio of the number of particles in each channel is $R_{s1,p} = N_{s1}/N_p$ and $R_{s2,p} = N_{s2}/N_p$, where N_{s1} and N_{s2} are the number of particles in the secondary channels and $N_p = 16$ is the number of particles in the primary channel. The spacing between channels d is marked in panel (a). (a) Two channels with $R_{s1,p} = 1.0$ (b) Two channels with $R_{s1,p} = 0.5$. (c) Three channels with $R_{s1,p} = 1.0$ and $R_{s2,p} = 1.0$. (d) Three channels with $R_{s1,p} = 1.0$ and $R_{s2,p} = 1.5$.

a rigid periodic substrate, such as atoms and molecules on surfaces [34], vortices in superconductors with periodic pinning arrays [35–37], and colloids interacting with 1D [38] or two-dimensional (2D) optical trap arrays [39], all of which can be viewed as physical realizations of the Frenkel-Kontrova model. These studies find that the coupling to the substrate or the effective pinning of the particles by the substrate is strongly enhanced when the ratio of the number of particles to the number of substrate minima is an integer or a rational fraction, as indicated by the appearance of peaks in the critical depinning force or enhanced ordering of the particles at the commensurate fillings. In our system, for the two channel geometry illustrated in Fig. 1 the particles in the secondary channel can be regarded as a distortable or moveable periodic pinning substrate for the particles in the primary channel, suggesting that enhanced drag or coupling could occur when the ratio of the number of particles in each channel is an integer or a rational fraction. The deformability of the substrate makes our proposed model distinct from Frenkel-Kontrova systems. Additionally, driven 1D and 2D commensurate-incommensurate systems often exhibit numerous dynamic behaviors within the incommensurate regimes, such as when localized vacancies or interstitials form soliton-like excitations which move more easily than the particles over the substrate [40, 41]. This suggests that similar phases may be possible in the coupled channel drag system we propose here, and we show that such phases do appear. We also show that when we make the system more complex by adding a third channel, a remarkable variety of commensuration effects and dynamic regimes occur such as multiple decoupling, recoupling, and slip transitions, all of which produce pronounced changes in the velocity response. It is even possible to realize negative drag effects where the particles in one of the channels move in the direction opposite to that of the applied drive.

The coupled channels system we propose could be realized in colloidal systems. The number of colloids in the different channels can be controlled readily by optical manipulation and the colloids in one channel could be driven with an external field, optically, or using microfluidics. Another possible realization of this system is in nanowires where 1D Wigner crystallization of the electrons has occurred; in this case, by altering the electron density, the particle lattice spacing in one wire could be varied with respect to that in an adjacent wire. Realizing such a system could have important implications for the study of 1D Wigner crystals since the appearance of commensuration effects would be strong evidence that Wigner crystal states are forming. In superconducting systems, the density of magnetic vortices is fixed by the externally applied magnetic field, so it would be difficult to create 1D channels that contain different linear densities of vortices; however, in certain layered systems an additional transverse magnetic field can be applied to create a second Josephson vortex lattice which can interact with the pancake vortices in the planes [42–44]. It has already been shown that using this technique it is possible to drive only one of the vortex species and induce a drag on the other vortex species [43, 44]. It should be possible to study fractional commensurate states in such a vortex system by examining how the drag effect changes when the ratio of the number of one type of vortices to the other is varied. A realization of three or more channels with varied numbers of particles in each channel should again be possible using colloidal systems or metallic wires. Further, a superconducting or nanowire system could be used in which each layer or channel has the same number of particles but differing amounts of quenched disorder. We note that there are previous studies of colloidal particles in 2D bilayers [45] where the particles in the layers are driven in opposite directions; however, these studies focused on an oscillatory order-disorder transition, not on the effects of commensuration on decoupling or the dynamic phases that we consider here for the case of 1D coupled channels.

The paper is organized as follows: In Section II, we describe our simulation method and sample geometry.

We consider two channels of particles in Section III and illustrate a drive-induced decoupling transition for commensurate channels in Section III A. In Section III B we describe the two step decoupling transition that occurs for incommensurate channels which contain vacancy or interstitial sites that can act like a second species of particle. The effects of finite temperature and finite size appear in Section III C. Section III D shows that the nonlinear response of the system can be exploited to create a ratchet effect, where ac motion in the driven channel induces dc transport in the drag channel. In Section IV we turn to samples with three channels. We show in Section IV A that when the driven channel is commensurate with the neighboring drag channel, four different types of coupled and decoupled flow can occur as the occupancy of the second drag channel is varied, including regimes of intermittent coupling. In Section IV B, the driven channel is incommensurate with the neighboring drag channel and we find a complex series of coupling-decoupling transitions that produce a significant amount of structure in the velocity-force curves. In Section IV C, we consider in detail the negative drag that can occur at incommensurate fillings when the particles in one of the drag channels move in the direction opposite to the particles in the driven channel. It is also possible for the outer channels to remain coupled while the central channel is decoupled, as described in Section IV D. In Section IV E we summarize all five of the dynamical phases and the negative drag by showing that they can be achieved in a single system. The paper concludes in Section V with a discussion and summary.

II. SIMULATION

We model interacting Yukawa particles confined to move along 1D channels as illustrated in Fig. 1. Each particle interacts with other particles in the same channel and with particles in adjacent channels. The separation between channels is $d = 2$ and, unless otherwise noted, there are $N_p = 16$ particles in the driven or primary channel with a lattice spacing a, where L is the length of the channel. The particles in the primary channel p are coupled to an applied external driving force F_D. For a two channel system, the drag or secondary channel s_1 contains N_{s1} particles, and the commensurability ratio is $R_{s1,p} = N_{s1}/N_p$. In a three channel system such as that shown in Fig. 1(c,d), the additional secondary channel s_2 is adjacent to s_1 but not to the primary channel p, and it contains N_{s2} particles, giving a commensurability ratio of $R_{s2,p} = N_{s2}/N_p$.

The particle motions evolve under overdamped dynamics where the colloids obey the following equation of motion:

$$\eta \frac{d\mathbf{R}_i}{dt} = \mathbf{F}_i^{pp} + \mathbf{F}_p^D \tag{1}$$

Here η is the damping constant, $\mathbf{R}_i$ is the location of particle i, and the repulsive particle-particle interaction force is $\mathbf{F}_i^{pp} = \sum_{j\neq i}^{N_v} -\nabla V(R_{ij})$. The potential has a Yukawa or screened Coulomb form of

$$V(R_{ij}) = \frac{E_0}{R_{ij}} e^{-\kappa R_{ij}} \tag{2}$$

with $E_0 = Z^{*2}/4\pi\epsilon\epsilon_0 a_0$, where ϵ is the solvent dielectric constant, Z^* is the effective charge, and $1/\kappa$ is the screening length. For colloidal systems, the length scale a_0 is on the order of a micron. We measure forces in units of $F_0 = E_0/a_0$ and time in units of $\tau = \eta/E_0$. In a typical case, the distance between particles in channel p is $a = 2.25$ while the distance between adjacent channels is $d = 1.125a$ and the screening length is $1/\kappa = 2d$, which is long enough to ensure strong coupling between the particles in all three channels. The driving force $F_p^D = F_D\hat{\mathbf{x}}$ is applied only to all the particles in the primary channel. We increase F_D from zero in small increments of δF_D, holding the drive at constant values for a fixed time interval during which we measure the velocity of the particles in each channel. We have carefully checked that our waiting times are long enough to eliminate transient effects. We use $\delta F_D = 0.001$ and a wait time of 10^5 simulation time steps. We impose periodic boundary conditions in the x-direction along the length of the channels. The velocity of the particles in the primary channel is given by V_p and the particle velocity in the secondary channels is given by V_{s1} and V_{s2}. We normalize all the velocities by the number of particles in each channel, $V_p = N_p^{-1}\sum_i^{N_p} \mathbf{v}_i$, $V_{s1} = N_{s1}^{-1}\sum_i^{N_{s1}} \mathbf{v}_i$, and $V_{s2} = N_{s2}^{-1}\sum_i^{N_{s2}} \mathbf{v}_i$.

III. TWO CHANNEL SYSTEMS

A. Coupling-Decoupling Transitions for Commensurate Channels

We first focus on the two channel system at commensurate filling with a particle ratio of $R_{s1,p} = 1.0$ and with $d/a = 0.67$. In Fig. 2(a) we plot V_p and V_{s1} together versus F_D. Both V_p and V_{s1} increase linearly with F_D for low F_D and have identical values, indicating that the motion in the two channels is locked. At $F_D = 2.125$, we find a transition to a partially decoupled state where V_{s1} monotonically decreases with increasing F_D while V_p continues to increase with F_D at a rate faster than the linear increase that occurred below the transition. The particles in s_1 are not completely decoupled from the primary channel since they still exhibit a nonzero velocity; since the particles in s_1 do not experience a driving force, they can move only due to interactions with the particles in p. Just above the decoupling transition, V_p increases with a square root form. The general shape of the velocity force curves in Fig. 2(a) is the same as that of the current-voltage curves obtained for superconducting transformer geometries [28–31], where the vortex velocities are proportional to the voltage and the applied

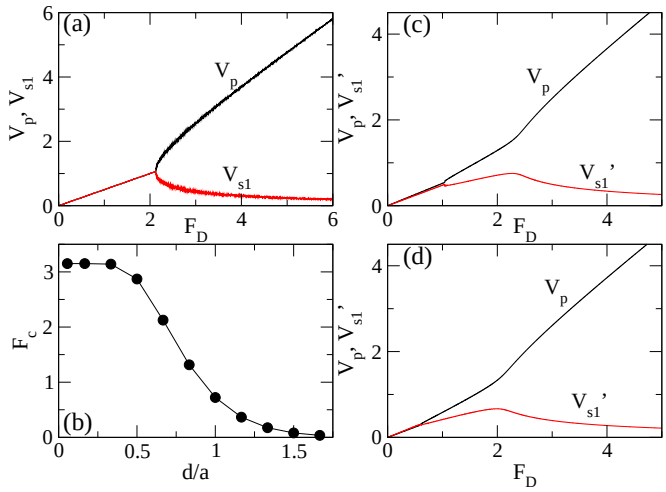

FIG. 2: (a) The average velocity in the primary channel V_p and the secondary channel V_{s1} vs F_D for a two channel system with $R_{s1,p} = 1.0$ and $d/a = 0.67$. The channels are locked for low F_D in the regime where V_p and V_{s1} increase linearly. At $F_D = 2.125$, there is a transition to a partially decoupled state where the particles in the secondary channel begin to slip, producing a decreasing V_{s1}. (b) The decoupling force F_c force vs d/a for the system in (a) with $R_{s1,p} = 1$, fixed $d = 2.0$, and a altered by changing the particle density. The decoupling transition drops to lower values of F_D as the particle density increases. (c) V_p (upper curve) and $V'_{s1} = N_p^{-1} \sum_i^{N_{s1}} \mathbf{v}_i$ (lower curve) vs F_D for the system in (a) but with $R_{s1,p} = 0.92$. Unlike the commensurate case in (a), the initial unlocking phase above $F_D = 1.04$ is associated with the slipping of vacancies in s_1, while at $F_D = 2.25$ there is a second unlocking transition above which all the particles in s_1 slip with respect to the particles in p. (d) V_p (upper curve) and V'_{s1} (lower curve) vs F_D for $R_{s1,p} = 1.08$, where the slipping at low drives is due to the presence of incommensurate particles.

current is proportional to the external force on the vortices in the primary channel. The current-voltage curves in the superconducting transformer system indicate that there is a drive-induced decoupling transition of the vortices in adjacent layers. In the vortex system, the vortex-vortex interaction between layers is attractive, so it is more intuitive why a finite vortex mobility persists in the secondary channel above decoupling. The results in Fig. 2(a) indicate that even when the particle-particle interactions are purely repulsive, a finite velocity in the secondary channel can be maintained at drives above the decoupling transition.

We measure the decoupling or unlocking force F_c as a function of d/a in a two channel system with $R_{s1,p} = 1.0$. The result is plotted in Fig. 2(b), where we fix $d = 2.0$ and vary a by changing N_p and N_{s1}. Here F_c decreases with increasing particle density. A similar effect occurs in layered vortex systems, where for higher fields or higher vortex densities the coupling between the layers is gradually reduced [31]. For the Yukawa system this effect can be attributed to the reduced size of the periodic potential that the particles in s_1 experience from the particles in p. Once the primary channel is in motion, the particles in s_1 shift to positions that are slightly behind the driven particles. As the drive increases, the size of this shift increases until the particles in p slip more than $0.5a$ ahead of the particles in s_1, producing the partial decoupling. When the particle density increases, the amount of shift required to pass the position $0.5a$ decreases since a decreases with increasing particle density in both channels.

B. Dynamics and Commensurability

In Fig. 2(c) we plot V_p and V'_{s1} for a two channel system with $R_{s1,p} = 0.92$, where the number of particles in s_1 is smaller than the number of particles in p. Here $V'_{s1} = N_p^{-1} \sum_i^{N_{s1}} \mathbf{v}_i$ is the velocity of the particles in s_1 normalized by N_p, the number of particles in p. For low F_D the channels are locked and all of the particles in the system move at the same velocity. The slope of V'_{s1} versus F_D is slightly smaller than the slope of V_p versus F_D in Fig. 2(c) due to the fact that $N_{s1} < N_p$. At $F_D = 1.04$ we observe a transition to a partially coupled state; however, this transition occurs at a drive well below the decoupling transition $F_c = 2.125$ shown for the commensurate system in Fig. 2(a). Additionally, just above $F_D = 1.04$, Fig. 2(c) indicates that the velocity-force curve does not have the characteristic square root shape found close to F_c in Fig. 2(a). For $F_D > 1.04$, V'_{s1} continues to increase with increasing F_D but with a smaller slope than in the locked regime. A second decoupling transition appears at $F_D = 2.25$. For $F_D > 2.25$, V'_{s1} decreases with increasing F_D and there is also a corresponding increase in the slope of V_p. The second decoupling transition occurs at a drive close to the value $F_c = 2.125$ where decoupling of the commensurate system occurs, as shown in Fig. 2(a). This indicates that the second decoupling transition for the incommensurate system is the same as the sole decoupling transition found in the commensurate system, where all the particles in s_1 begin to slip with respect to the particles in p. The two step decoupling transition for the incommensurate system appears due to the presence of vacancies in s_1. At commensuration, all of the particles in s_1 are located within potential minima created by the spacing of the particles in p. Below commensuration, a fraction of the sites in this periodic potential are empty, producing effective vacancies in s_1. In the locked phase at $F_D < 1.04$, all the particles in s_1 move at the same velocity as the particles in p. At the first decoupling transition, the vacancies in s_1 begin to slip with respect to the particles in p. This can be viewed as a depinning transition. Every time a vacancy slips, only one of the particles in s_1 slips with respect to p while the remaining particles in s_1 stay locked with p. As a result, most of the particles in s_1 continue to increase in velocity with increasing F_D. For drives above the second decoupling transition, all of the particles in s_1 slip with respect to p

and the slipping is no longer dominated by the motion of vacancies.

In Fig. 2(d) we plot V_p and V'_{s1} versus F_D for the same system in Fig. 2(c) but with $R_{s1,p} = 1.08$, where $N_{s1} > N_p$ so that a few incommensurate particles appear in s_1. The overall shape of the velocity-force curve in this case is very similar to that for $R_{s1,p} = 0.92$ shown in Fig. 2(c), with a first decoupling occurring at a lower drive of $F_D = 0.6$ than that for $R_{s1,p} = 0.92$, and a second decoupling transition occurring close to $F_D = 2.0$. Here the incommensurations in s_1 form doubly occupied sites in the periodic potential created by the particles in p. At $R_{s1,p} = 0.92$ when there are vacancies in s_1, slipping of a particle adjacent to a vacancy occurs because the particle is able to move closer to the barrier separating two minima in the periodic potential. This is because the force the particle experiences on one side from a neighboring particle in s_1 is not compensated due to the missing particle at the vacancy site. As a result, there is an extra force of the order of $F^{pp}(a)$ on the slipping particle, where a is the lattice constant of the particles in p. For the doubly occupied sites at $R_{s1,p} = 1.08$, a similar situation occurs; however, the slipping particle in s_1 is located at a doubly occupied site and feels an uncompensated force from the other particle located within the same site. The extra force in this case is $F_{pp}(a')$, where $a' < a$ in order for the site to be doubly occupied. Thus, $F_{pp}(a') < F_{pp}(a)$, so the initial decoupling transition occurs at a lower value of F_D for samples with $R_{s1,p} > 1$ that have incommensurations than for samples with $R_{s1,p} < 1$ that contain vacancies.

The appearance of multiple decoupling transitions just below and above commensuration and only one transition at commensuration is similar to the single and multiple depinning transitions observed in vortex systems [40] and colloidal systems [46] with periodic potentials at and near commensuration. In these 2D systems, at the matching filling of 1 particle per substrate minimum there is a single transition from a pinned state to a flowing state, while at fillings slightly away from commensuration, well-defined vacancies or interstitial particles appear which are highly mobile and depin at a lower external drive than the commensurate particles. The 2D systems are generally more complicated and allow for more than two depinning transitions near but not at commensuration [40]; however, as in our 1D case, it is the presence of two types of particles, the commensurate particles and the interstitial or vacancy sites, that produce the multiple depinning transitions. There are some important differences between our two channel system and the 2D vortex and colloidal systems. Our system contains no fixed periodic substrate so there is no pinned phase; however, there is a moving fully coupled state which is analogous to the pinned state. The regime in which the vacancies or incommensurations slip is then analogous to the depinning transitions of interstitials or vacancies, and the high driving phases at which all the particles are slipping corresponds to the completely depinned regime in the 2D systems.

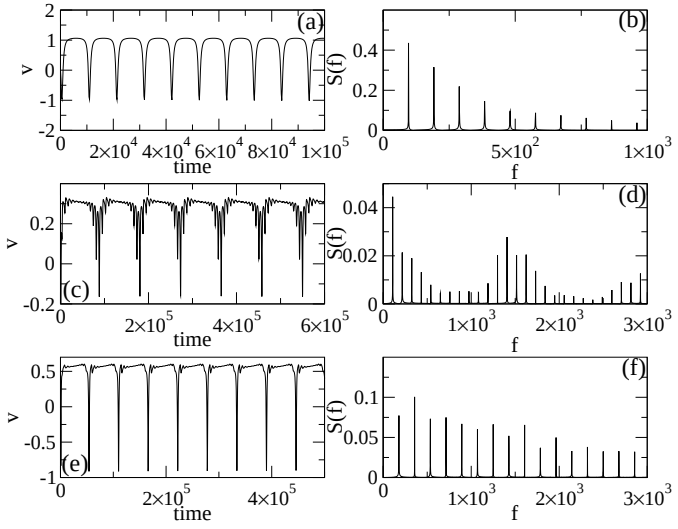

FIG. 3: (a) The velocity v of a single particle in s_1 vs time for the commensurate system in Fig. 2(a) at $R_{s1,p} = 1.0$ and $F_D = 2.25$. (b) The Fourier transform $S(f)$ of the signal in panel (a) shows a well-defined characteristic frequency. (c) $v(t)$ for a system with $R_{s1,p} = 1.08$ at $F_D = 0.65$. (d) The corresponding $S(f)$ shows that there are two frequencies present. (e) $v(t)$ for a system with $R_{s1,p} = 0.92$ at $F_D = 1.1$. (f) The corresponding $S(f)$ shows the presence of two frequencies.

In order to show more clearly that the particles in s_1 are experiencing a periodic potential produced by the particles in p and that there are two effective types of particles in s_1 away from commensuration, in Fig. 3(a) we plot the time trace of the velocity $v(t)$ of a single particle in s_1 for the system in Fig. 2(a) at $R_{s1,p} = 1.0$ in the locked phase at $F_D = 2.25$. The value of $v(t)$ is nearly constant except during the periodic slip events, during which v drops briefly below zero indicating that the particle temporarily moves backwards. In Fig. 3(b) we show the Fourier transform $S(f)$ of $v(t)$ highlighting the presence of a single characteristic frequency determined by the slipping events. In the locked phase, there is no high-frequency oscillation of the velocity of any of the particles. In Fig. 3(c) we plot $v(t)$ for the system with $R_{s1,p} = 1.08$ from Fig. 2(d) at $F_D = 0.65$ where the channels are not completely locked but where V'_{s1} is still increasing with increasing F_D, and in Fig. 3(d) we show $S(f)$ for the same data. There are now two frequencies present. The lower frequency is produced by the same slipping events that occurred for the commensurate system in Fig. 3(a,b), while the higher frequency originates from the motion of the incommensuration through s_1. In Fig. 3(e,f) we plot $v(t)$ and $S(f)$ for a sample with $R_{s1,p} = 0.92$ at $F_D = 1.1$. Again, there are two characteristic frequencies. The lower frequency is associated with the same slipping events shown previously, while the higher frequency is produced by the motion of a vacancy through s_1, rather than by the motion of an incommen-

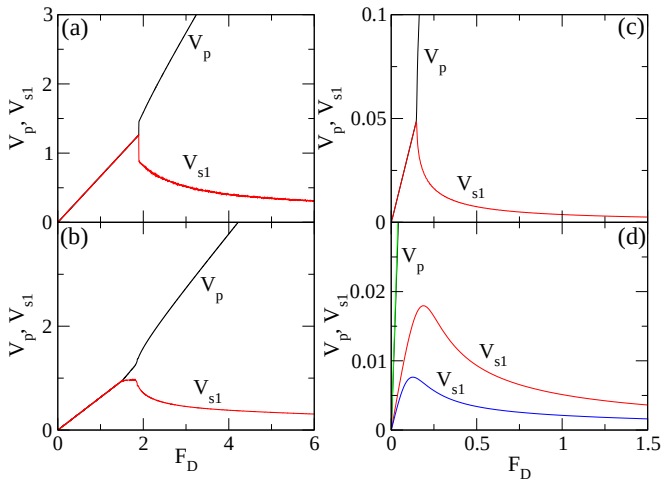

FIG. 4: V_p (upper curve) and V_{s1} (lower curve) vs F_D for the two channel system from Fig. 2(a). (a) At $R_{s1,p} = 0.5$, there is a single transition from the completely coupled state to the partially decoupled state. (b) At $R_{s1,p} = 0.58$ there are two transitions. The first decoupling transition occurs when the incommensurations begin to slip while the other particles in s_1 remain locked with p. (c) At $R_{s1,p} = 2.0$ there is a single transition out of the locked phase. (d) At $R_{s1,p} = 1.92$ (upper V_{s1} curve) and $R_{s1,p} = 2.08$ (lower V_{s1} curve) there is no locked phase, but there is still a local maximum in V_{s1} which is higher for $R_{s1,p} = 1.92$.

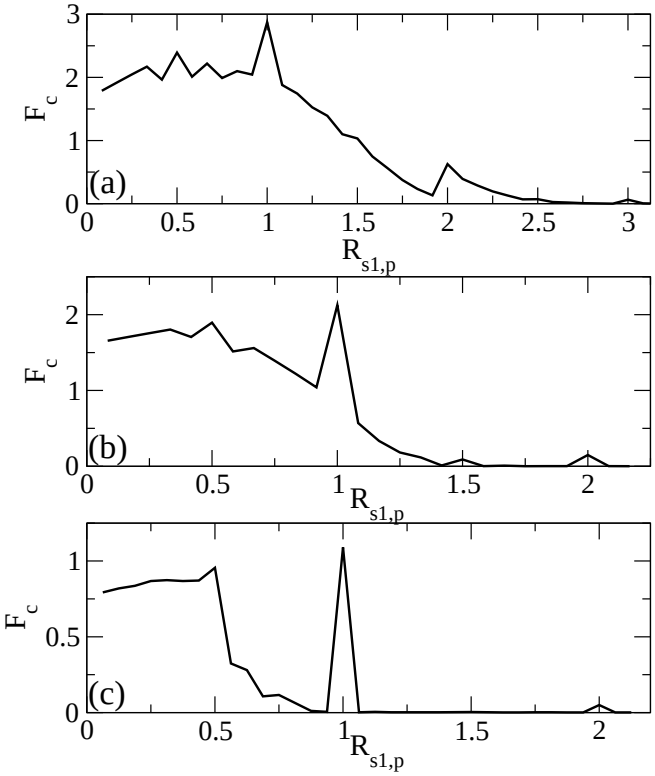

FIG. 5: The force F_c at the transition from the locked to unlocked phase vs $R_{s1,p}$ in two channel samples with different values of a. (a) At $d/a = 0.44$, commensuration peaks occur at $R_{s1,p} = 1.0$, 2.0, and 3.0. Fractional peaks and anomalies appear at $R_{s1,p} = 0.5$, 1.5, and 2.5. (b) At $d/a = 0.67$, there are commensuration peaks at $R_{s1,p} = 0.5$, 1.0, 1.5, and 2.0. (c) At $d/a = 1.0$, the strongest commensuration peaks appear at $R_{s1,p} = 1$ and 0.5.

suration.

The two stage decoupling process is most pronounced for fillings close to $R_{s1,p} = 1.0$, but the same effects appear near certain fractional ratios. For example, in Fig. 4(a) we plot V_p and V_{s1} versus F_D for a sample with $R_{s1,p} = 0.5$ which has a single sharp decoupling transition at $F_D = 1.9$. Just above this filling at $R_{s1,p} = 0.58$, shown in Fig. 4(b), there is an initial decoupling transition of the incommensurations near $F_D = 1.5$ into a state where V_{s1} still increases with increasing F_D but with a greatly reduced slope. A second decoupling transition appears at $F_D = 1.8$, and above this drive V_{s1} decreases with increasing F_D. In this case, incommensurations appear with respect to the particle configuration that occurs at $R_{s1,p} = 0.5$. There is a single frequency associated with the motion of the particles in s_1 for $R_{s1,p} = 0.5$, while for the incommensurate case of $R_{s1,p} = 0.58$, two frequencies are present. This trend persists for higher values of $R_{s1,p}$ as shown in Fig. 4(c) at $R_{s1,p} = 2.0$. Here there is a single sharp decoupling transition, while just below and just above this filling at $R_{s1,p} = 1.92$ and $R_{s1,p} = 2.08$, Fig. 4(d) shows that the locking phase is absent but that a strong local maximum in V_{s1} appears at $F_D = 0.19$ for $R_{s1,p} = 1.92$ and at $F_D = 0.125$ for $R_{s1,p} = 2.08$.

By performing a series of simulations for varied $R_{s1,p}$, we determine the location F_c of the transition from complete locking to a decoupled state and map out where the commensuration effects occur. In Fig. 5(a), we plot the decoupling force F_c versus $R_{s1,p}$ for a two channel sample with $d/a = 0.44$, which falls in the strong coupling regime in Fig. 2(b). There are peaks in F_c at $R_{s1,p} = 1.0$, 2.0, and 3.0, along with submatching peaks at $R_{s1,p} = 1/3$, 1/2, and 2/3. Additionally, weaker anomalies appear at $R_{s1,p} = 1.5$ and 2.5. In Fig. 5(b) we show F_c versus $R_{s1,p}$ for a sample with $d/a = 0.67$. The value of F_c at the commensurate filling of $R_{s1,p} = 1.0$ is lower for the $d/a = 0.67$ sample than for the $d/a = 0.44$ sample. Figure 5(b) also has clear peaks in F_c at $R_{s1,p} = 2.0$, 1.5, and 0.5, while above $R_{s1,p} = 2.0$ within our resolution there are no peaks or regions where the system is locked. In the regions with $F_c = 0$ where the locked phase is absent, the second decoupling transition still appears at higher drives and can be detected as the point at which V_{s1} changes from increasing to decreasing with increasing F_D. For higher particle densities and fixed d, the commensurability effects still persist as shown in Fig. 5(c) for $d/a = 1.0$. Here, peaks in F_c occur at $R_{s1,p} = 0.5$, 1.0, and 2.0.

The appearance of the commensuration effects at integer and fractional fillings suggests that this system ex-

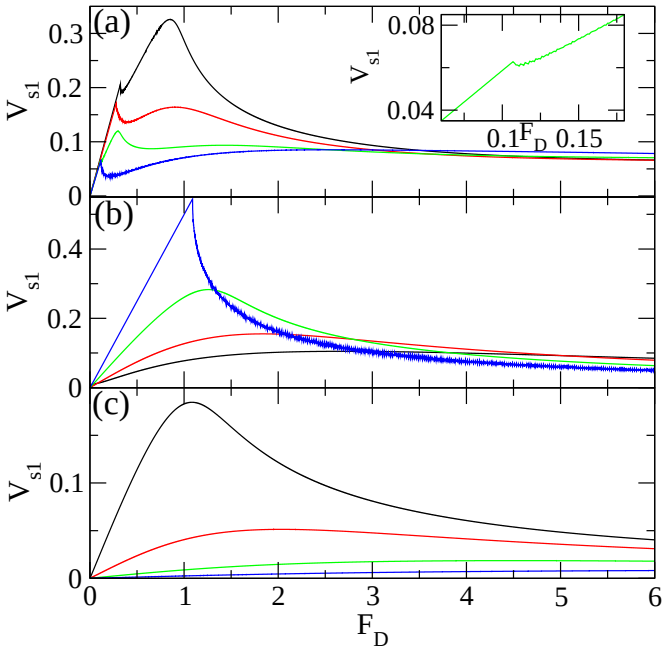

FIG. 6: V_{s1} vs F_D for the system in Fig. 5(b) with $d/a = 0.67$. (a) $R_{s1,p} = 0.562$, 0.625, 0.6875, and 0.75, from top to bottom. Inset: Detail of the $R_{s1,p} = 0.6875$ curve from the main panel. (b) $R_{s1,p} = 0.8125$, 0.875, 0.9375, and 1.0, from bottom to top. (c) $R_{s1,p} = 1.0625$, 1.125, 1.1875, and 1.25, from top to bottom.

hibits the same behavior found for the depinning of repulsively interacting particles on a 1D fixed periodic potential; however, there are several differences between the two systems. For particles on a fixed periodic potential, the depinning force F_c at fields where the particle-particle interactions cancel due to symmetry equals the maximum value of the pinning force F_p so that $F_c = F_p$ at fillings 1/12, 1/8, 1/6, 1/4, 1/2, and 1.0. For the drag system shown in Fig. 5, this does not occur and there is even a trend for F_c to increase at the lowest fillings. This is because the substrate potential created by the particles in p is not fixed but can distort since the particles in either channel can shift. At $R_{s1,p} = 1.0$, the periodic potential is fairly rigid due to the matching of the particle positions in p and $s1$, and any distortion of the particles in p is energetically unfavorable. In contrast, at very low fillings such as $R_{s1,p} = 0.125$, the particles in p distort near the locations of the particles in s_1 in order to create a localized lowering of the density in p above each particle in s_1. As a result, the particles in s_1 no longer experience the same periodic potential from p that was present for the commensurate case of $R_{s1,p} = 1.0$. Even at $R_{s1,p} = 0.5$, the particles in p can distort, reducing the strength of the coupling to the particles in s_1.

In order to better understand the changes in dynamics at the different fillings, in Fig. 6 we plot V_{s1} as a function of F_D for varied $R_{s1,p}$ in a system with $d/a = 0.67$. At $R_{s1,p} = 0.5$, a single decoupling transition occurs and V_{s1} is a monotonically decreasing function. For $R_{s1,p} = 0.562$ and 0.625, shown in Fig. 6(a), there is a clear double peak structure in V_{s1} with one peak falling at the depinning of the incommensurations and the second peak appearing at the unlocking transition. At $R_{s1,p} = 0.6875$ in Fig. 6(a), there is now a three peak structure in V_{s1}. The first peak, shown in the inset of Fig. 6(a), falls at the transition out of the completely locked phase at $F_D = 0.11$. The second and largest peak is at $F_D = 0.3$, while a third broad peak also appears that is centered at $F_D = 1.45$. The broad peak is the remnant of the second peak in V_{s1} found for $R_{s1,p} = 0.562$ and 0.625; with increasing $R_{s1,p}$, this peak broadens and the center shifts to higher values of F_D. For $0.11 < F_D < 0.3$, the particles in s_1 are almost completely locked but there is a single incommensuration which has begun to slip. For $R_{s1,p} = 0.75$, the initial peak is lost and the decoupling transition peak now falls at $F_D = 0.11$. There is also a very broad maximum centered at $F_D = 4.0$. Another interesting feature is that at higher F_D such as at $F_D = 6.0$, V_{s1} for $R_{s1,p} = 0.75$ is higher than V_{s1} at the lower values of $R_{s1,p}$, even though at low F_D $R_{s1,p}$ showed the lowest value of V_{s1}. This suggests that at high values of F_D, additional drag is produced by the interaction between the incommensurations in s_1 and the particles in p.

In Fig. 6(b) we plot V_{s1} versus F_D for $R_{s1,p} = 0.8125$, 0.875, 0.9375, and 1.0. The maximum value of V_{s1} increases as $R_{s1,p}$ increases toward $R_{s1,p} = 1.0$ and the broad maximum in V_{s1} sharpens and shifts toward lower F_D. Here, $R_{s1,p} = 1.0$ has the lowest value and $R_{s1,p} = 0.8125$ has the highest value of V_{s1} at $F_D = 6.0$. In Fig. 6(c) we show V_{s1} versus F_D for $R_{s1,p} = 1.0625$, 1.125, 1.1875, and 1.25. For these values of $R_{s1,p}$ there is no completely locked phase; however, there is still a peak feature in V_{s1} for $R_{s1,p} = 1.0625$ and 1.125 which broadens and shifts to higher F_D for increasing $R_{s1,p}$. At $R_{s1,p} = 2.0$ a locked phase reappears and the shape of V_{s1} versus F_D is very similar to the curve shown for $R_{s1,p} = 1.0$.

In Fig. 7(a) we plot V_{s1} versus $R_{s1,p}$ at a fixed drive of $F_D = 6.0$ for the system in Fig. 6 with $d/a = 0.67$. Larger values of V_{s1} indicate that the particles in s_1 are exerting a larger drag on the particles in p. Here, peaks fall at $R_{s1,p} = 0.45$ and $R_{s1,p} = 0.8$, rather than at the values $R_{s1,p} = 0.5$ and $R_{s1,p} = 1.0$ where peaks appeared in F_c in Fig. 5(b). This shows that at high drives, the drag by the s_1 particles is the most effective away from the commensurate fillings. The curves shown in Fig. 6 indicate that if V_{s1} were measured at a lower value of F_D, the peaks in Fig. 7(a) would shift closer to $R_{s1,p} = 0.5$ and 1.0.

In vortex systems with 2D periodic pinning arrays, experiments have shown that the pinning is enhanced at the matching fields as indicated by dips in the resistivity for low applied drives. For vortices that are strongly driven, however, the resistivity dips were found to shift away from the integer matching fields [47]. The interpretation was that at the matching fields in the highly

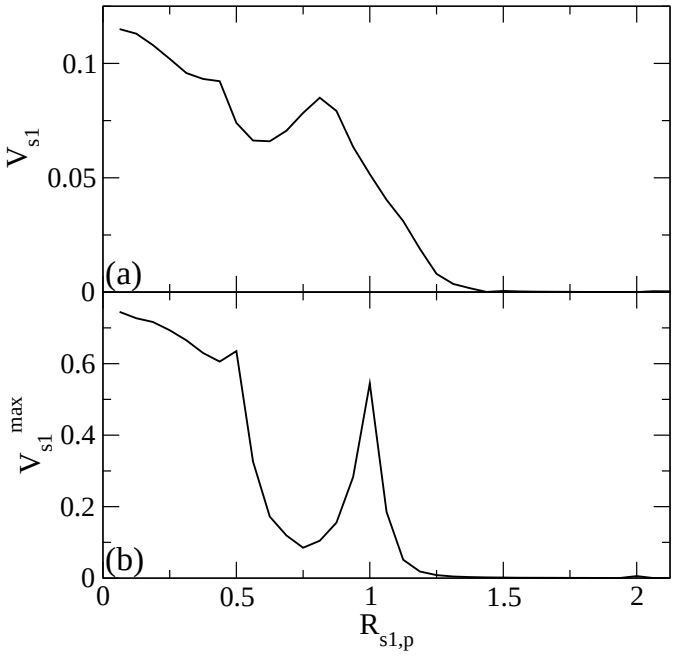

FIG. 7: V_{s1} vs $R_{s1,p}$ at $F_D = 6.0$ for the two channel system with $d/a = 0.67$. Here the peaks appear not at the commensurate fields of $R_{s1,p} = 1.0$ and $R_{s1,p} = 0.5$ but at $R_{s1,p} = 0.8$ and $R_{s1,p} = 0.45$. (b) V_{s1}^{max} vs $R_{s1,p}$ obtained for each filling at the F_D where V_{s1} reaches its maximum value. The peak centered at $R_{s1,p} = 1.0$ is much broader than the peak in F_c at $R_{s1,p} = 1.0$ shown in Fig. 5(b).

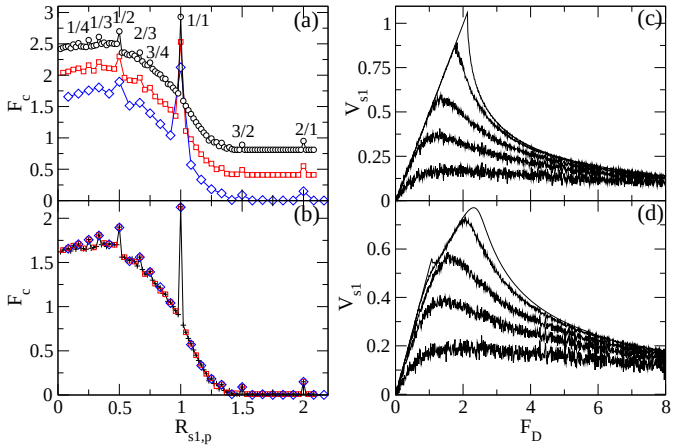

FIG. 8: (a) F_c vs $R_{s1,p}$ for the system with $d/a = 0.67$ from Fig. 5(b) of length L (diamonds), $2L$ (squares, curve shifted up by 0.4), and $4L$ (circles, curve shifted up by 0.8). For the larger systems, higher order fractional peaks appear at $R_{s1,p} = 1/4$, $1/3$, $1/2$, $2/3$, $3/4$, and $3/2$. (b) The same data plotted without vertical shifts, for system sizes of L (diamonds), $2L$ (squares), and $4L$ (plus signs). Connecting lines are drawn only for the $4L$ system. The curves overlap exactly and the values of F_c are unaffected by system size. (c,d) V_{s1} vs F_D for the $4L$ system from (a) at (c) $R_{s1,p} = 1.0$ and (d) $R_{s1,p} = 0.896$ for temperatures of $T = 0.0$, 0.22, 0.88, 2.0, and 4.5, from top to bottom. The decoupling transition drops to lower F_D with increasing T, while the drag effects persist up to high temperatures.

driven system, the vortices form a very ordered moving commensurate state, while at the incommensurate fields the moving state is not as well ordered and thus the effectiveness of the pinning increases away from commensuration at high drives. Although the disorder in the incommensurate state causes the system to begin slipping at a lower drive for incommensurate fields, at high drives the disordered state experiences more fluctuations than the ordered state which induce some additional drag.

In Fig. 7(b) we plot V_{s1}^{max} versus $R_{s1,p}$. Here the measurement of V_{s1}^{max} is performed not at a fixed F_D but at the F_D where V_{s1} reaches its maximum for each value of $R_{s1,p}$. In this case, a strong peak in V_{s1}^{max} appears at $R_{s1,p} = 1.0$. This peak is wider than the peak in F_c at $R_{s1,p} = 1.0$ in Fig. 5(b) due to the fact that the maximum value of V_{s1} increases as $R_{s1,p} = 1.0$ is approached, as shown in Fig. 6(b,c).

C. Finite Size and Temperature Effects

To determine whether further higher order submatching effects in $R_{s1,p}$ can be resolved for larger systems and whether the values of F_D at which the unlocking transitions occur change with system size, we consider the system at $d/a = 0.67$ from Fig. 5(b) and analyze F_c for samples of size $2L$ and $4L$. Here we hold a fixed by increasing N_p to 32 and 64, respectively. In Fig. 8(a) we plot F_c versus $R_{s1,p}$ for samples of size L, $2L$, and $4L$, with the curves shifted vertically for clarity. In the larger samples, there are clearly fractional peaks falling at $R_{s1,p} = 1/4$, $1/3$, $1/2$, $2/3$, $3/4$, and $3/2$. The $4L$ sample even shows some evidence of a peak at $R_{s1,p} = 1/8$. We expect that for even larger systems, even more fractional peaks will appear but that the higher order peaks will be increasingly weak in size, similar to the behavior of fractional peaks observed in other systems such as vortices on periodic substrates [35, 36]. In Fig. 8(b) we plot the same data without vertical shifts to show that the depinning thresholds for the three systems overlap exactly; only the resolution is changed by the system size. We find no changes in the velocity-force curves as the size of the sample is increased, indicating that the system sizes we are studying capture the essential behavior. We also find a similar lack of dependence on sample size for the three layer systems that are described in Section IV. We note that for commensurate-incommensurate systems such as the Frenkel-Kontrova model [33], submatching effects theoretically occur for all rational values of m/n, where m is the number of particles and n is the number of substrate minima. In the Frenkel-Kontrova model, true incommensurate behavior occurs only for systems of infinite size at irrational filling ratios. In our system the higher order submatching effects are destroyed due to the fact that we do not have a fixed substrate; in-

stead, the effective substrate experienced by the particles in one channel due to the presence of particles in the neighboring channel is able to distort. As a result, our system does not map directly onto commensurate-incommensurate systems such as the Frenkel-Kontrova model, although it displays several similarities with such models as we have shown.

In an experimental realization of the system we propose, such as with colloids confined to channels, thermal effects will be present. To test the stability of the different regimes we observe against thermal perturbations, we have performed simulations with the $4L$ system with $d/a = 0.67$ at $R_{s1,p} = 1.0$ and $R_{s1,p} = 0.896$ at finite temperature. We use the same procedure employed in previous works to model the thermal fluctuations [48]. We add a Langevin noise term F_i^T to the equation of motion with the properties $\langle F_i^T(t)\rangle = 0$ and $\langle F_i^T(t)F_j^T(t')\rangle = 2\eta k_B T\delta_{ij}\delta(t-t')$. Fig. 8(c) illustrates V_{s1} versus F_D at $R_{s1,p} = 1.0$ and Fig. 8(d) shows V_{s1} versus F_D at $R_{s1,p} = 0.896$ for $T = 0.0$, 0.22, 0.88, 2.0, and 4.5. As the temperature increases, the value of F_c decreases until for $T > 2.0$ the locked phase has almost completely vanished; however, drag effects on the secondary channel continue to persist up to much higher temperatures. For $R_{s1,p} = 0.896$, the locking phase is lost at lower T than for $R_{s1,p} = 1.0$ due to the fact that the effective incommensurations are more mobile and hence require a smaller level of thermal fluctuations to escape from the potential minima. These results show that the drag and locking features described for the zero temperature system should persist under finite temperature provided that the thermal fluctuations are not excessively strong.

Possible experimental realizations of the two channel system include modified versions of the colloidal experiments which have already been performed on coupled one-dimensional channels [9]. Colloidal systems are subject to thermal fluctuations and hydrodynamic interactions which can arise in the surrounding fluid. We showed above that the dynamic phases are robust against moderate thermal fluctuations. There is ongoing discussion regarding how the inclusion of hydrodynamic effects would impact the dynamics of driven colloidal systems. Recent two-dimensional simulations of an electrophoretically driven charged colloidal system similar to the one we consider showed that when the charge on the colloids are sufficiently strong, the dynamical behavior of the system is not altered by the addition of hydrodynamic interactions [49]. Due to the good agreement that has been found between numerous simulations of driven colloid systems in which hydrodynamic effects are neglected and the actual behavior of driven colloids in experiment, we expect that at least some of the features that we describe should be observable in a colloidal realization of this system. Another possible realization would be to generalize the recent experiments performed with dusty plasmas interacting with a one-dimensional groove to create what are termed Yukawa chains [21]. If more than one groove were created in the substrate, it should be possible to couple two or more of the Yukawa chains, to use a laser to drive one of the chains, and then to analyze the response of the secondary chain. In this case inertial effects could modify the behavior since dusty plasma systems are generally not in the overdamped limit.

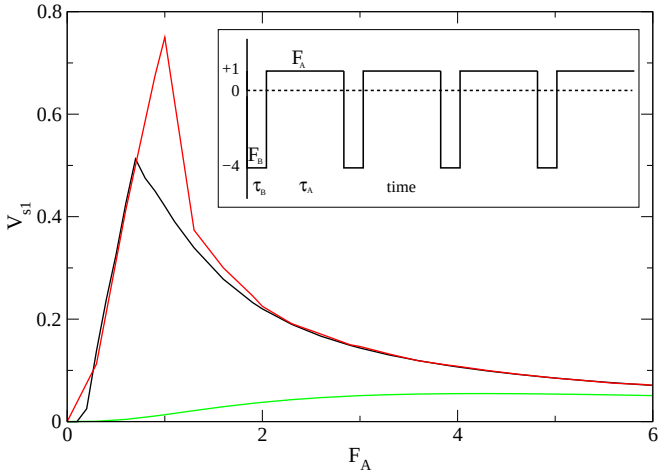

FIG. 9: Inset: Schematic of the ac force applied to p. Each period τ is divided into two parts. A force F_A is applied in the positive direction for a duration τ_A, then a force F_B is applied in the negative direction for a duration τ_B, with the condition that $F_B/F_A = \tau_A/\tau_B = 4.0$. Main panel: Induced dc velocity V_{s1} averaged over multiple ac drive periods vs F_A for a two channel system with $d/a = 0.67$ under the applied ac drive shown schematically in the inset. Upper curve: $R_{s1,p} = 1.0$; middle curve: $R_{s1,p} = 0.75$; lower curve: $R_{s1,p} = 1.25$. Here the ratchet effect reaches its maximum value for $R_{s1,p} = 1.0$. Within this range of F_A, $V_p = 0$ when averaged over an ac drive period.

D. Ratchet Effect With ac Drives

We next show that when the particles in p are driven with an ac drive, it is possible to generate a net dc motion of the particles in s_1 or a ratchet effect. Ratchet effects produced by applied ac drives have been studied extensively in systems of particles interacting with asymmetric substrates [50]; however, it is also possible to create a ratchet effect in the absence of an asymmetric substrate when the ac drive has certain asymmetries and when the response of the system is nonlinear [42–44, 51]. This type of ratchet has been realized in systems with two interacting species of superconducting vortices such as when Josephson vortices couple to pancake vortices [42–44], as well as in interacting binary colloidal systems where only one colloid species couples to an external driving field and produces a rectification of the other colloid species [51].

Here we consider an ac square drive applied only to p. The period τ of the square drive is divided unevenly

into two parts as illustrated in the inset of Fig. 9. In part A, we apply a force $\mathbf{F}_D = F_A\hat{\mathbf{x}}$ in the positive direction for a duration τ_A, while in part B we apply a force $\mathbf{F}_D = -F_B\hat{\mathbf{x}}$ in the negative direction for a duration $\tau_B = \tau - \tau_A$. In selecting F_A and F_B, we impose the condition $F_A\tau_A - F_B\tau_B = 0$ so that there is no net dc drive. If the response of the system is perfectly linear, this drive will not generate a net dc motion of the particles in either channel. On the other hand, if the coupling between s_1 and p is nonlinear, it is possible to induce a dc motion of the particles in s_1 by applying this ac drive to the particles in p. If both F_A and F_B are below the first decoupling transition F_c, the motion of the particles in both channels is completely locked, the response is perfectly linear, and there is no ratchet effect. If $F_A < F_c$ and $F_B > F_c$, a net dc drift of the particles in s_1 will occur since the particles in s_1 remain completely locked with the particles in p during part A of the drive cycle, but during part B of the cycle the particles in s_1 are partially decoupled and do not move all the way back to their starting position by the end of the cycle.

In Fig. 9 we illustrate the ratchet effect which produces a finite positive value of V_{s1} under the ac drive described above. We fix $F_B/F_A = 4.0$ and $d/a = 0.67$, and plot the time-averaged V_{s1} versus F_A for $R_{s1,p} = 0.75$, 1.0, and 1.25. For low F_A, V_{s1} starts small but rapidly grows with increasing F_A, reaching a sharp peak for $R_{s1,p} = 0.75$ and $R_{s1,p} = 1.0$. As F_A increases above this peak, V_{s1} gradually decreases with increasing F_A since the drag effect becomes smaller for higher drives as shown in Fig. 2(a). For $R_{s1,p} = 1.25$, the ratchet effect is strongly reduced but still persists, indicating that the ratchet effect should be a robust feature for all fillings. In all cases there is no induced dc flow of the particles in p. Our system can be regarded as containing two species of particles: the directly driven particles in p, and the undriven particles in s_1 that experience a drag from the particles in p. It would be very interesting to look for a similar ratchet effect in coupled quantum wires in the regime where Wigner crystallization may be occurring. This could be achieved by applying an ac drive of the type illustrated in the inset of Fig. 9 to one wire and determining whether a dc response is induced in the second wire.

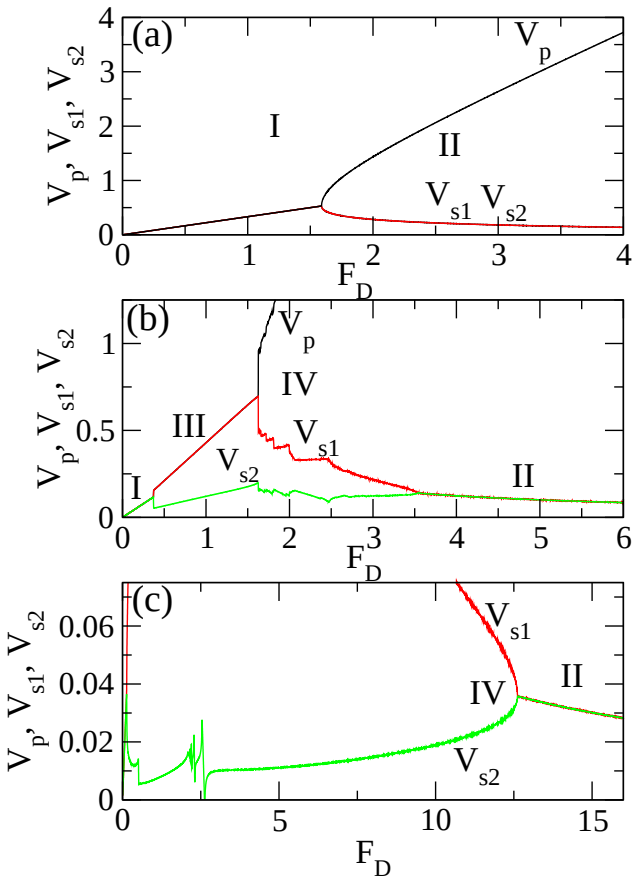

FIG. 10: The velocities V_p, V_{s1}, and V_{s2} vs F_D for a three channel system with $d/a = 0.67$, $R_{s1,p} = 1.0$, and varied $R_{s2,s1}$. (a) At $R_{s2,s1} = 1.0$ there is a single transition from the locked region I to region II where the particles in s_1 and s_2 remain locked with each other but partially decouple from the particles in p. (b) At $R_{s2,s1} = 1.16$ there is a transition from the locked region I to region III where the particles in $s1$ and p lock together but the particles in s_2 partially decouple. In region IV all three channels are unlocked, while at high F_D the system enters region II when the particles in s_1 lock with the particles in s_2 but are partially decoupled from the particles in p. (c) At $R_{s2,s1} = 1.5$ the transition between regions IV and II occurs at a much higher value of F_D.

IV. THREE CHANNEL SYSTEMS

A. Coupling-Decoupling Transitions for Partial Commensuration

We next consider a system with three channels of particles where only the top channel is subjected to a driving force. We measure the velocities in each channel, denoted by V_p, V_{s1}, and V_{s2}, for particle ratios of $R_{s1,p} = N_{s1}/N_p$, $R_{s2,p} = N_{s2}/N_p$, and $R_{s2,s1} = N_{s2}/N_{s1}$. For the commensurate case when all channels contain the same number of particles, $R_{s1,p} = R_{s2,p} = R_{s2,s1} = 1.0$, the behavior is the same as in the two channel case at commensuration. There is a single decoupling transition from region I, the completely locked phase, to region II, where the particles in s_1 and s_2 remain locked with each other but are partially decoupled from the particles in p. This is illustrated in the plot of V_p, V_{s1}, and V_{s2} versus F_D in Fig. 10(a) for a sample with $d/a = 0.67$, $R_{s1,p} = 1.0$, and $R_{s2,s1} = 1.0$. The decoupling between the primary and the secondary channels occurs at $F_D = 1.75$. The value of F_D at decoupling is lower than for a sample containing only two channels since the primary channel must now drag twice as many secondary particles.

In Fig. 10(b) we plot the channel velocities versus F_D for a sample with $R_{s1,p} = 1.0$ but with more particles in s_2, $R_{s2,s1} = 1.16$. For $F_D < 0.37$ the system is in the

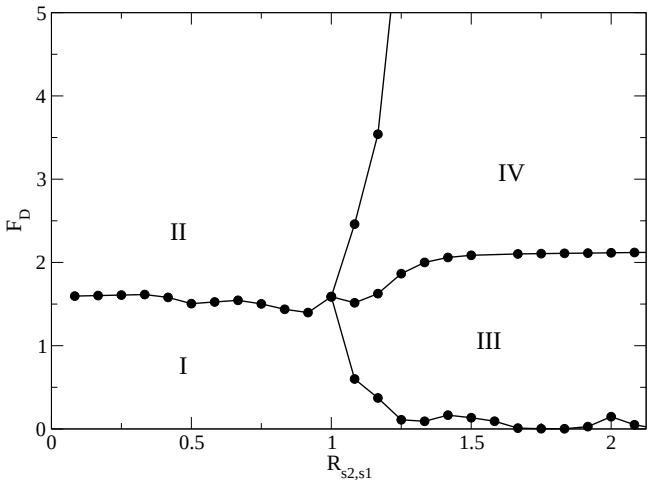

FIG. 11: The three channel dynamic phase diagram for F_D vs $R_{s2,s1}$ in the system from Fig. 10 with $R_{s1,p} = 1.0$. The locations of regions I, II, III, and IV are marked. Peaks appear in the value of F_D at which region I ends for the commensurate ratios of $R_{s2,s1} = 1.0$ and $R_{s2,s1} = 2.0$

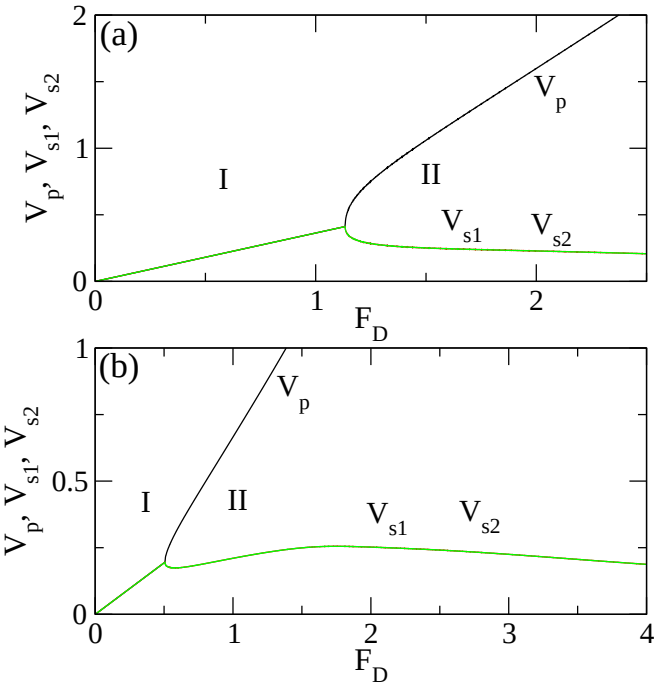

FIG. 12: V_p, V_{s1}, and V_{s2} versus F_D for a three channel system with $R_{s1,p} = 0.75$ and varied $R_{s2,p}$. (a) At $R_{s2,p} = 1.0$ there is a single transition from region I to region II. (b) At $R_{s2,p} = 0.833$, the single region I-region II transition is accompanied by an additional secondary maximum in V_{s1} and V_{s2} centered at $F_D = 1.75$.

completely locked region I, while for $0.37 \leq F_D < 1.625$ the particles in p and s_1 remain locked but the particles in s_2 partially decouple. We term this range of F_D region III, and in this region V_{s2} still increases with increasing F_D. For $1.625 \leq F_D < 3.56$, all three of the channels are unlocked; we call this region IV. Within region IV, the velocity curves contain numerous small steps associated with the intermittent coupling of the particles in s_1 and s_2. At the low F_D end of region IV, V_{s1} and V_{s2} both decrease with increasing F_D, but for $2.7 < F_D < 3.56$, V_{s2} begins to increase with increasing F_D until V_{s1} and V_{s2} join at the recoupling transition into region II. Once the system is in region II, both V_{s1} and V_{s2} decrease monotonically with increasing F_D.

For samples with $R_{s1,p} = 1.0$ but with increasing $R_{s2,s1}$, the general features of the velocity force curves are the same as Fig. 10(b), but the transition into region II is pushed to higher F_D. This is illustrated in Fig. 10(c) where we plot V_p, V_{s1}, and V_{s2} versus F_D for a system with $R_{s1,p} = 1.0$ and $R_{s2,s1} = 1.5$. Here region II does not appear until $F_D = 12.5$. Fig. 10(c) also shows more clearly the increase in V_{s2} just below the onset of region II. For samples with $R_{s1,p} = 1.0$ and $R_{s2,s1} < 1.0$, only regions I and II occur and the velocity force curves have the same form as the curves illustrated in Fig. 10(a).

In Fig. 11 we map out the dynamic phase diagram for a three channel system with $R_{s1,p} = 1.0$ and varied $R_{s2,s1}$. The value of F_D at which a transition out of region I occurs shows commensurate peaks at $R_{s2,s1} = 1.0$ and $R_{s2,s1} = 2.0$, while the region III-region IV transition falls at a roughly constant value of $F_D = 2.1$. The region II-region IV transition line shifts to slightly higher F_D with increasing $R_{s2,s1}$. This trend continues for F_D values higher than those shown in Fig. 11, until at $R_{s2,s1} = 2.0$ the II-IV transition drops to a value of $F_D = 7.5$ (not shown in the figure). These results indicate that commensurability effects also occur in the moving phases at high F_D.

B. Dynamics for Increased Incommensuration

In Figs. 12 and 13 we plot V_p, V_{s1}, and V_{s2} versus F_D for a three channel system with $R_{s1,p} = 0.75$ and varied $R_{s2,p}$. At $R_{s2,p} = 1.0$, shown in Fig. 12(a), there is a single decoupling transition from region I to region II at $F_D = 1.14$. For $R_{s2,p} < 1.0$, only regions I and II occur; however, V_{s1} and V_{s2} may contain additional features such as those shown in Fig. 12(b) for $R_{s2,p} = 0.833$. Here the decoupling into region II occurs near $F_D = 0.5$ which is significantly lower than the location of the I-II transition in the $R_{s2,p} = 1.0$ case. There is also a secondary maximum in V_{s1} and V_{s2} near $F_D = 1.7$ which is similar to the secondary maximum that appears in V_{s1} at incommensurate fillings in the two channel system. At $R_{s2,p} = 1.25$ in Fig. 13(a), the sample first transitions at $F_D = 0.8$ from region I to region III, where the particles in s_1 and p are locked but the particles in s_2 are partially decoupled. At $F_D = 0.86$ the sample enters region IV where all the channels are unlocked. The III-IV transition is also marked by a change in sign of the slope of the velocity-force curves for both of the sec-

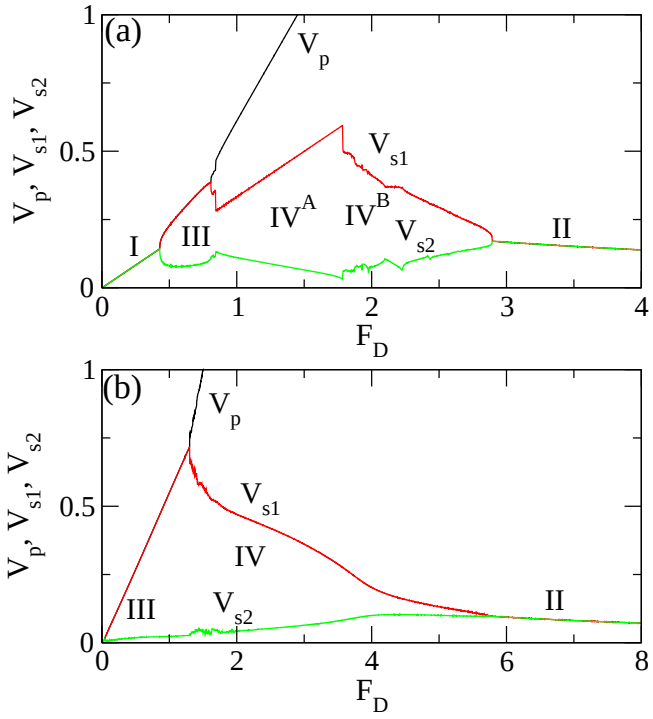

FIG. 13: V_p, V_{s1}, and V_{s2} versus F_D for a three channel system with $R_{s1,p} = 0.75$ and varied $R_{s2,p}$. (a) At $R_{s2,p} = 1.25$, region I is followed by a transition into region III. In region IV^A, all the channels are unlocked, V_{s1} increases with increasing F_D, and V_{s2} decreases with increasing F_D. In region IV^B, V_{s1} decreases with increasing F_D and V_{s2} increases with increasing F_D. There is a transition to region II at high F_D. (b) At $R_{s2,p} = 1.583$, there is a small window of region I at low F_D which is not highlighted on the figure. There is a transition directly from region III to region IV^B, with region IV^A absent.

ondary channels. In Fig. 13(a) we divide region IV into two subregions. Just above the III-IV transition we have region IV^A in which V_{s1} increases with increasing F_D while V_{s2} decreases with increasing F_D. In region IV^B this behavior is reversed and V_{s1} decreases while V_{s2} increases with increasing F_D. When the particles in s_1 and s_2 recouple, a transition from region IV^B to region II occurs and both V_{s1} and V_{s2} decrease with increasing F_D. There are two distinct subregions of region IV only for $1.0 < R_{s2,p} < 1.5$. For $R_{s2,p} > 1.5$, only region IV^B appears, as shown in Fig. 13(b) for $R_{s2,p} = 1.583$ where the III-IV^B transition falls at $F_D = 1.3$. There is a small window of region I that occurs at very low F_D which is not highlighted in the figure.

Figure 14 shows the F_D versus $R_{s2,p}$ phase diagram for the system in Fig. 12 with $R_{s1,p} = 0.75$ and $d/a = 0.67$. Here, the value of F_D at which region I ends passes through peaks at the commensurate values of $R_{s2,p} = 0.25$, 0.5, 0.75, 1.0, and 1.75, with a weaker peak at $R_{s2,p} = 2.0$. The pronounced peak at $R_{s2,p} = 0.75$ also corresponds to the commensurability condition $R_{s2,s1} = 1.0$. Region IV^A first appears for $R_{s2,p} = 1.0$ and vanishes at $R_{s2,p} = 1.5$, which is the $R_{s2,s1} = 2.0$ filling. The value of F_D at which the transition from region II to region IV^B occurs increases with increasing $R_{s2,p}$, except at $R_{s2,p} = 1.5$ where the II-IV^B transition suddenly drops to a lower value of F_D.

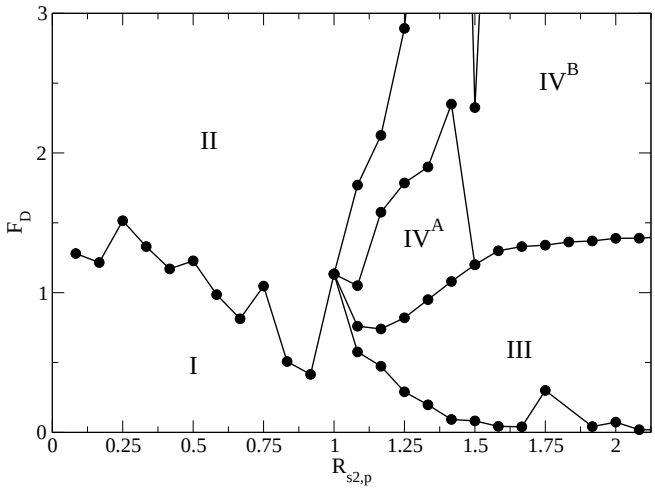

FIG. 14: The dynamic phase diagram of F_D vs $R_{s2,p}$ for the system in Fig. 12 with $R_{s1,p} = 0.75$.

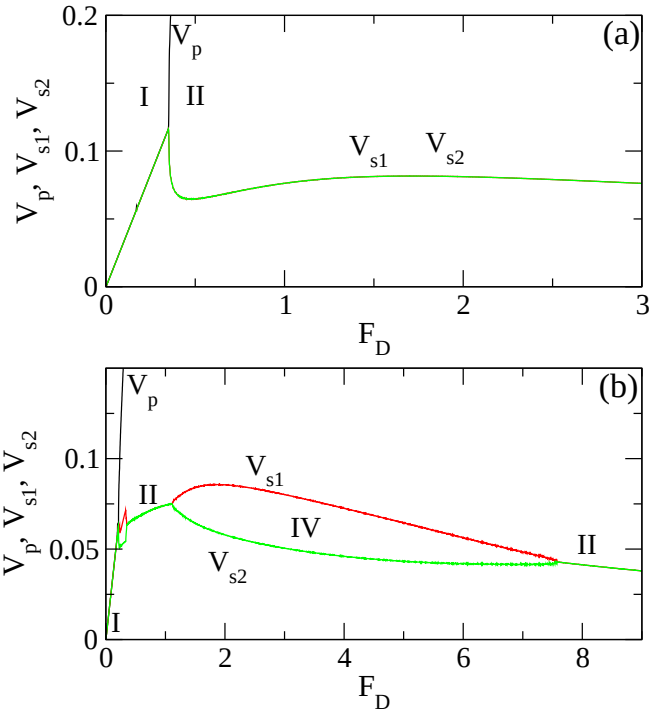

FIG. 15: V_p, V_{s1}, and V_{s2} vs F_D for the three channel system with $R_{s1,p} = 1.25$ and $d/a = 0.67$. (a) At $R_{s2,s1} = 0.6$ only regions I and II are present. (b) At $R_{s2,s1} = 0.86$ the system enters region II more than once.

In Fig. 15(a) we plot V_p, V_{s1}, and V_{s2} versus F_D for a three layer system with $R_{s1,p} = 1.25$ at $R_{s2,s1} = 0.6$.

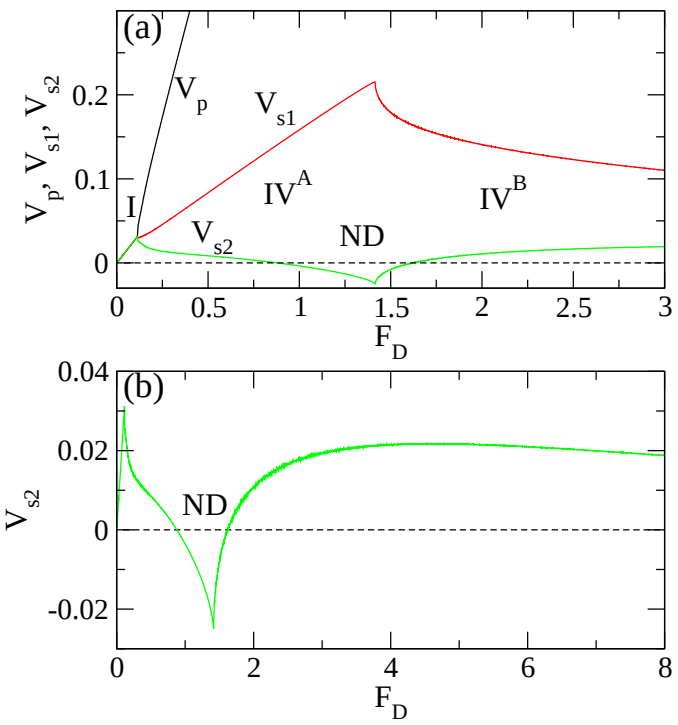

FIG. 16: V_p, V_{s1}, and V_{s2} versus F_D for the three channel system with $R_{s1,p} = 1.25$. (a) At $R_{s2,s1} = 1.067$, there is a transition from the locked region I to region IV^A. This is followed by a transition to region IV^B. V_{s2} drops below zero in the region marked ND where negative drag occurs. (b) V_{s2} vs F_D from (a) showing the region of negative velocities as well as the existence of a local maximum at higher F_D.

Only regions I and II are present, and there is an additional second broad maximum in V_{s1} and V_{s2} centered near $F_D = 1.5$. In general, for $R_{s1,p} = 1.25$ and $R_{s2,s1} < 0.8$ or $R_{s2,s1} > 1.0$, only regions I and II appear. For $0.86 \leq R_{s2,s1} < 1.0$, region II is broken into two sections by an intermediate transition to region IV, as shown in Fig. 15(b) for $R_{s2,s1} = 0.86$. The system passes from region I to region II, then enters region IV and finally returns to region II at high F_D.

The dynamic phase diagrams presented here give a concise description of the velocity-force curves as the system parameters are varied. Such dynamic phase diagrams have been widely used in studies of driven particle systems such as vortices in type-II superconductors [40]; however, they have no connection with equilibrium phase diagrams obtained from systems in the thermodynamic limit. Having more than three phase transition lines meet in an equilibrium phase diagram would be highly unusual; however, in the nonequilibrium dynamic phase diagram, having more than three lines meet has no special implications since the lines do not represent true phase transition lines. Whether nonequilibrium systems can undergo true phase transitions that resemble equilibrium phase transitions is currently a topic of active study and is beyond the scope of this manuscript to address. The appearance of multiple phases typically occurs when the s_1 and s_2 channels can become unlocked with each other. For $R_{s1,s2} < 1.0$, incommensurations in the form of holes are present in one channel; however, the mobility of the holes is less than that of the interstitials which arise when $R_{s1,s2} > 1.0$.

C. Negative Drag

For $1.0 < R_{s2,s1} \leq 1.6$ and fixed $R_{s1,p} = 1.25$, we show that a negative drag effect can occur for the particles in s_2. During negative drag, the particles in s_2 move in the direction opposite to the direction in which the particles in p are being driven. Negative drag has been observed in coupled 1D wires where Wigner crystallization is expected to occur [32]. In Fig. 16(a) we plot V_p, V_{s1}, and V_{s2} for a three channel system with $R_{s2,s1} = 1.067$. Here the sample is in the locked region I for $F_D < 0.1$. For $0.1 < F_D < 1.4$, region IV^A appears with all three channels decoupled, V_{s1} increasing with increasing F_D, and V_{s2} decreasing with increasing F_D. At $F_D = 1.4$ there is a cusp in both V_{s1} and V_{s2} at the onset of region IV^B. The cusp also marks the point at which V_{s2} reaches its maximum negative value. In Fig. 16(a) this is labeled ND for the negative drag region, which extends from $1.0 < F_D < 1.6$. In Fig. 16(b) we plot V_{s2} alone versus F_D for the system in Fig. 16(a) showing the negative drag effect more clearly and also showing the presence of a local maximum in V_{s2} at $F_D = 4.5$. Above this drive, V_{s2} decreases with increasing F_D but remains positive.

In Fig. 17 we plot the time dependent velocity $v(t)$ of a single particle in each of of the three channels for the system in Fig. 16 at $F_D = 1.36$ where the particles in s_2 undergo negative drag. The velocity of the particle in p is always positive and is composed of two frequencies. The velocity of the particle in s_1 again shows two frequencies and drops below zero for a portion of each cycle; however, the overall time average of the velocity remains positive. The particle in s_2 also experiences a combination of positive and negative velocities; however, the negative velocity portion of each cycle is greater than the positive velocity portion, and the particle takes a step backwards at the negative cusp in each cycle. It was previously demonstrated that a system driven by two external ac drives can exhibit a ratchet effect in the absence of an asymmetric substrate [52–54]. In our three channel system, when N_p, N_{s1}, and N_{s2} are all different, the dynamical potential produced by the particles in p and s_1 acts effectively like two ac driving signals for the particles in s_2. In some cases, the interfering frequencies of these ac drives can create a local potential maximum in s_2 that is moving in a direction opposite to F_D. As F_D is further increased, the different ac frequencies shift, increasing or decreasing the ratchet effect until for high enough F_D the coupling between s_2 and the particles in the other channels becomes so weak that a ratchet effect can no longer occur.

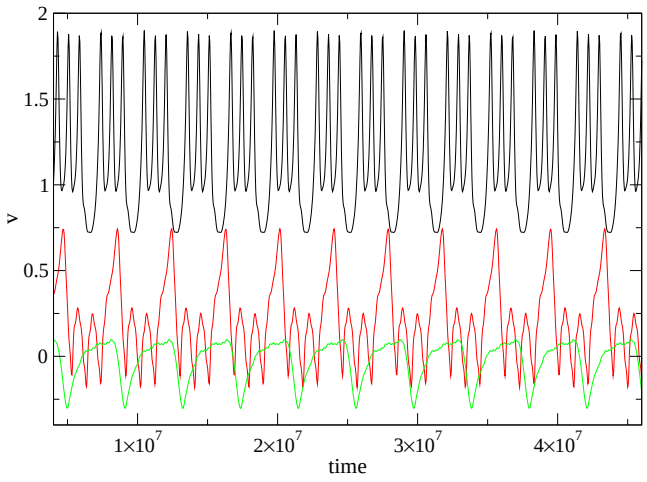

FIG. 17: The time dependent velocity v of a single particle in each of the channels for the system in Fig. 15 at $F_D = 1.36$. Upper curve: p; middle curve: s_1; lower curve: s_2. The velocity of the particle in p exhibits two frequencies and is always positive. The velocity of the particle in s_1 also shows two frequencies and passes below zero for a portion of each cycle, but the time averaged velocity remains positive. The particle in s_2 spends a larger fraction of each cycle moving in the negative direction, producing a negative time averaged velocity.

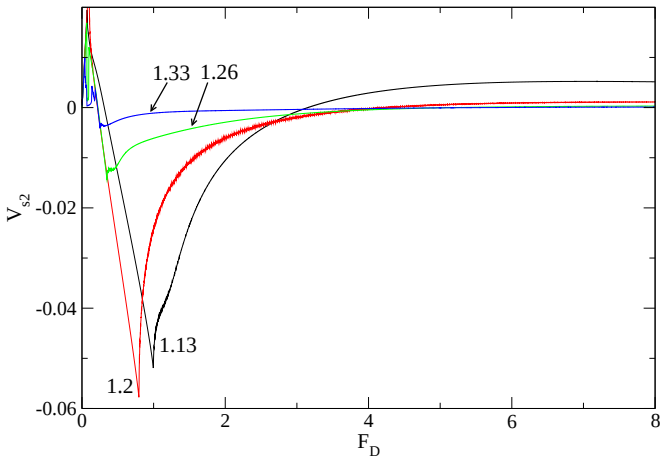

FIG. 18: V_{s2} vs F_D for the system in Fig. 15 at $R_{s2,s1} = 1.13$, 1.2, 1.26, and 1.33, as labeled. The largest negative maximum occurs for $R_{s2,s1} = 1.2$.

In Fig. 18 we plot only the normalized velocities V_{s2} versus F_D for three channel samples with $R_{s1,p} = 1.25$ and $R_{s2,s1} = 1.13$, 1.2, 1.26, and 1.33. This shows how the magnitude and extent of the negative drag region changes with filling. The negative velocity is maximum for $R_{s2,s1} = 1.2$ and gradually decreases with increasing $R_{s2,s1}$. In Fig. 19(a), the plot of F_D versus $R_{s2,s1}$ is marked with the region ND where negative drag occurs. The dashed line indicates the location of the the transitions between region IV^A and region IV^B. This transition also coincides with the maximum negative value of V_{s2} for fixed $R_{s2,s1}$. In Fig. 19(b) we show $|V_{s2}|$ taken at the IV^A-IV^B transition as a function of $R_{s1,s2}$, showing that the overall maximum negative value of V_{s2} occurs at $R_{s1,s2} = 1.2$.

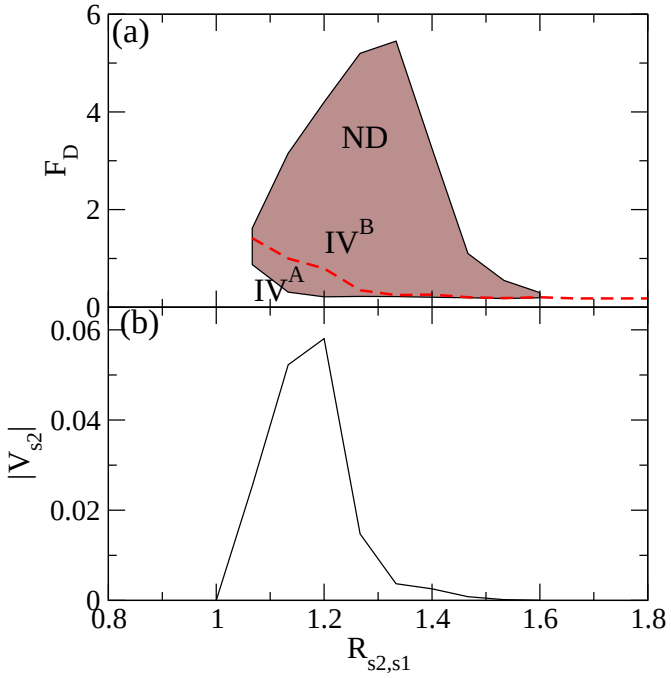

FIG. 19: (a) F_D vs $R_{s2,s1}$ for the system in Fig. 15. The shaded region marked ND indicates where the negative drag for the particles in s_2 occurs. Dashed line: The transition between regions IV^A and IV^B. The largest negative maximum of V_{s2} falls on this line. (b) $|V_{s2}|$, the magnitude of the largest negative maximum in V_{s2} in the negative drag region, vs $R_{s2,s1}$ for the same system.

In Fig. 20 we show the dynamic phase diagram of F_D versus $R_{s2,s1}$ for the three channel system with $R_{s1,p} = 1.25$ and $d/a = 0.67$. There are peaks in the transition out of region I at $R_{s2,s1} = 0.4$, 0.6 0.8, 1.2, and 1.8. These peaks correspond to $R_{s2,p} = 0.5$, 0.75, 1.0, 1.5, and 2.25, with the most prominent peak appearing at $R_{s2,p} = 1.0$. For $R_{s2,s1} < 0.8$ the system exhibits only regions I and II, while for $0.8 < R_{s2,s1} \leq 1.0$, the transition from region I to region II is followed by a transition into region IV^B at higher F_D. At even higher $F_D > 7.7$, not shown in the figure, the line marking the transition from region II to region IV^B changes curvature and approaches $R_{s2,s1} = 1.0$ with increasing F_D. As a result, for $0.8 < R_{s1,s2} \leq 1.0$ there is a high-drive transition from region IV^B back to region II (not shown) when the particles in s_1 and s_2 recouple, similar to the region IV-region II transition illustrated at high F_D in Fig. 15(b). At $R_{s2,s1} = 1.0$, the dashed line indicates the transition from region IV^B to region IV^A. For $R_{s2,s1} > 1.5$, the upper region IV^A-region IV^B transition saturates to the line $F_D = 0.18$. Near $R_{s2,s1} = 1.0$, the upper IV^A-IV^B tran-

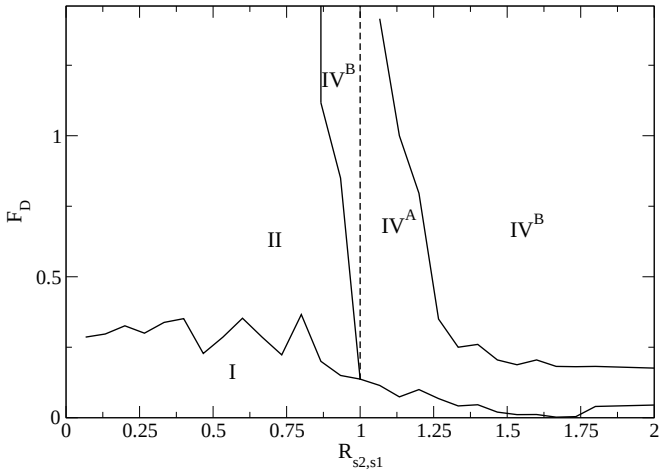

FIG. 20: The dynamic phase diagram of F_D vs $R_{s2,s1}$ for the three channel system with $R_{s1,p} = 1.25$ and $d/a = 0.67$. The prominent commensurate peak in the region I-region II transition at $R_{s2,s1} = 0.8$ also corresponds to the commensurability condition of $R_{s2,p} = 1.0$. The dashed line indicates that at $R_{s2,s1} = 1.0$, the system crosses from region IV^B to region IV^A. At higher F_D (not shown), the line marking the end of region IV^A approaches $R_{s2,s1}$ from above, and once it reaches $R_{s2,s1}$, region IV^A disappears. Also at higher F_D (not shown), the line marking the beginning of region IV^B approaches $R_{s2,s1}$ from below, producing a transition from region IV^B to region II with increasing F_D.

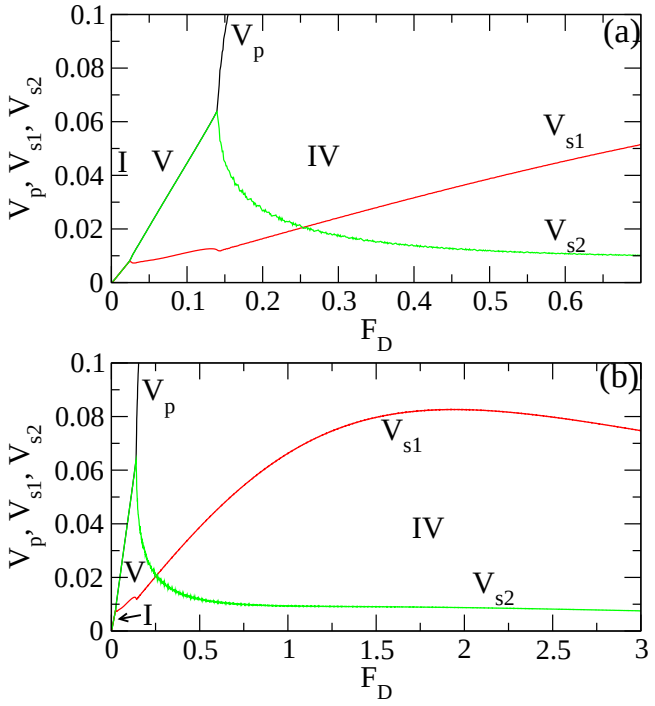

FIG. 21: V_p, V_{s1}, and V_{s2} vs F_D for a three channel system with $R_{s1,p} = R_{s2,s1} = 1.133$, $R_{s2,p} = 1.0$, and $d/a = 0.94$. Here we observe a transition from region I to region V, where the particles in p and s_2 remain locked to each other but the particles in s_1 are unlocked. This is followed by region IV, when the particles in s_2 unlock from the particles in p and V_{s1} increases with increasing F_D. (b) The same data plotted over a larger range of F_D shows that V_{s1} reaches a plateau at $F_D = 1.9$ and then decreases with increasing F_D.

sition line approaches $R_{s2,s1}$ from above with increasing F_D, and when the transition reaches $R_{s2,s1}$ below $F_D = 2$ (not shown in the figure), region IV^A disappears. For $R_{s2,s1} > 1.0$, we find no recoupling transition back into region II within the range $F_D \leq 15.0$. Additionally, region III, where the particles in p and s_1 are locked but the particles in s_2 are unlocked, never occurs at all. We have performed additional simulations for varied $R_{s1,p} > 1.0$ other than the value $R_{s1,p} = 1.25$ shown in Fig. 20 and find that the same sequence of regions illustrated in the figure appears in each case.

D. Unlocking of the Central Channel

Another possible dynamic phase has the particles in p and s_2 locked with each other while the particles in s_1 are unlocked. We term this region V, and expect it to occur when the average interaction between the particles in p and s_2 is greater than the interaction between the particles in p and s_1 even though the distance between s_1 and p is shorter than the distance between s_2 and p. In Fig. 21(a) we show an example of the occurrence of region V in a system with $R_{s1,p} = 1.133$, $R_{s2,s1} = 1.133$, $R_{s2,p} = 1.0$, and $d/a = 1.06$. In this case the p and s_2 channels are commensurate. At low F_D, the system is in the locked phase I. As F_D increases, the particles in s_1 decouple from the particles in s_2 and p, which remain locked to each other. This is indicated by the region in which V_{s1} splits away from V_p and V_{s2} and increases at a diminished rate with increasing F_D. At $F_D = 0.14$, the particles in s_2 also decouple from p and the system enters region IV, in which V_{s2} monotonically decreases with increasing F_D. After the particles in s_2 decouple from the particles in p, the coupling between the particles in p and s_1 is increased, as indicated by the increase in the slope of V_{s1} at the onset of region IV. V_{s1} continues to increase with increasing F_D throughout region IV and even rises above V_{s2} for $F_D > 0.2$. In Fig. 21(b) we plot the same data over a larger range of F_D to show that V_{s2} reaches a maximum value near $F_D = 1.9$ before turning over and beginning to decrease with increasing F_D.

The results in Fig. 21 show that it is possible to achieve region V in certain situations, such as when the particles in p and s_2 are commensurate. In general it is very difficult to obtain region V behavior in our system. The coupling between the particles in p and those in s_2 is relatively weak since the distance between p and s_2 is equal to the screening length. As a result, particles in s_2 experience a weak interaction only with those particles in p that lie directly above their positions, and interact much more weakly still with the other particles in

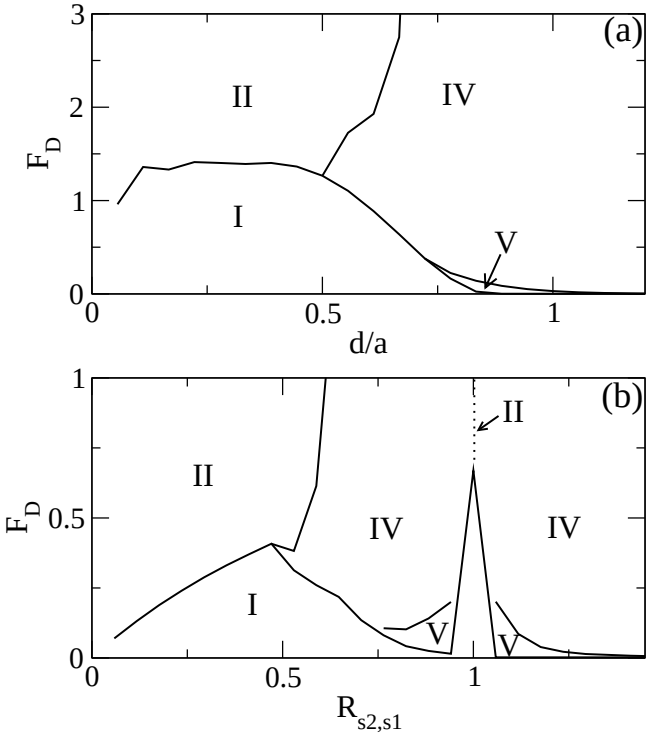

FIG. 22: (a) The dynamic phase diagram of F_D vs d/a for a system with $R_{s1,p} = 1.133$, $R_{s2,p} = 1.0$, and $R_{s2,s1} = 0.883$. Here region V occurs for $d/a > 0.75$. (b) The dynamic phase diagram of F_D vs $R_{s2,s1}$ for a system with $R_{s2,p} = 1.0$ and $d/a = 1.06$. Commensurability peaks appear in the transition out of region I at $R_{s2,s1} = 1.0$ and $R_{s2,s1} = 0.5$. Region V appears on either side of the commensuration peak at $R_{s2,s1} = 1.0$. The dashed line indicates that at $R_{s2,s1} = 1.0$, the system passes directly from region I to region II.

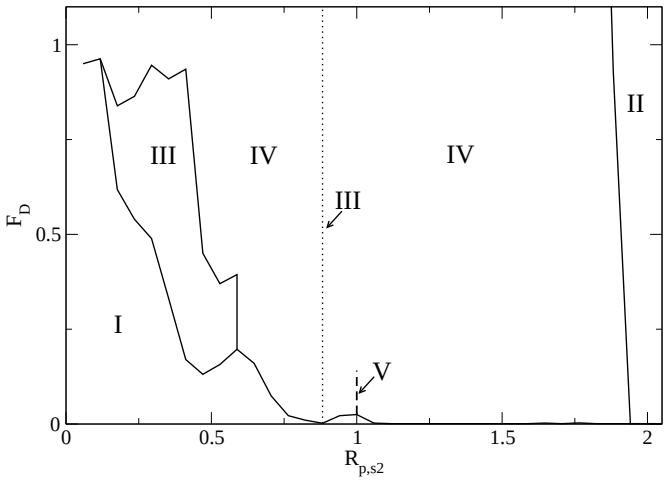

FIG. 23: The dynamic phase diagram of F_D vs $R_{p,s2} = N_p/N_{s2}$ for a system in which N_p is varied. Here $R_{s2,s1} = 1.133$ and $d/a_{s1} = 0.833$, where a_{s1} is the spacing of the particles in s_1. All five regions appear as marked. Region IV can be subdivided into regions IV^A and IV^B as discussed previously, but for clarity this subdivision is omitted here. Commensuration peaks at the transition out of region I appear at $R_{p,s2} = 1.0$ and at $R_{p,s2} = 0.58825$; the latter corresponds to the commensurability condition of $R_{s1,p} = 2/3$. The dotted line at $R_{p,s2} = 0.882$ corresponds to $R_{s1,p} = 1.0$ where the system transitions directly from region I to region III. A transition from region III to region IV occurs for this filling at $F_D = 1.25$ (not shown). At $R_{p,s2} = 1.0$ the transition from region I to region V is marked by the thick dashed line. For this filling, region V ends at $F_D = 0.141$ and is followed by region IV. The transition from region IV to region II at high $R_{p,s2}$ continues to rise to higher values of F_D as $R_{p,s2}$ decreases over a range of F_D larger than shown in the figure.

p. (Note that we do not cut off the interaction at the screening length, but continue to compute the weak interaction out to longer distances.) This suggests that for different screening lengths $1/\kappa$ and interchannel distances d the coupling between particles in p and particles in s_2 could be enhanced, producing a more widespread occurrence of region V and leading to additional commensuration effects. The densities of the particles in the channels, and not merely the ratio of their numbers, also plays an important role in determining which dynamical regions will appear. For higher particle density (smaller a), the couplings between the particles in all the channels are reduced, as demonstrated for the two channel case in Fig. 2(b). Even if the effective coupling between the particles in p and those in s_2 is strengthened by altering the density of the particles in the channel, this coupling must still be stronger than the coupling between the particles in p and those in s_1 in order for region V to appear.

In order to understand where region V occurs as a function of the coupling between the channels, in Fig. 22(a) we plot the dynamic phase diagram of F_D versus d/a for a system with fixed $R_{s1,p} = 1.133$, $R_{s2,p} = 1.0$, and $R_{s1,s2} = 0.883$. For small d/a the system passes directly from region I to region II. At $d/a = 0.5$ a window of region IV opens between regions I and II. Region V first appears at $d/a = 0.75$, and gradually disappears for increasing $R_{s2,s1}$. We next consider the case of $d/a = 1.06$ and $R_{s2,p} = 1.0$ for varied $R_{s2,s1}$, as shown in Fig. 22(b). Here, there is a pronounced commensurability peak in the transition out of region I at $R_{s2,s1} = 1.0$, where all the channels contain the same number of particles. At $R_{s2,s1} = 1.0$ the system passes directly from region I to region II. In windows just below and just above $R_{s2,s1} = 1.0$ we find that region V appears and is accompanied by a transition to region IV with increasing F_D. The width of region V grows as $R_{s2,s1} = 1.0$ is approached from either side. For $R_{s2,s1} > 1.0$, region V gradually decreases in size with increasing $R_{s2,s1}$, while for $R_{s2,s1} < 0.75$, region V vanishes completely. For $0.5 < R_{s2,s1} < 0.75$ the system transitions from region I into region IV with increasing F_D and eventually enters region II at high F_D (not shown). For $R_{s2,s1} < 0.5$ there is a only a single transition from region I to region II. A second commensurate peak in the transition out of region I appears at $R_{s2,s1} = 0.5$.

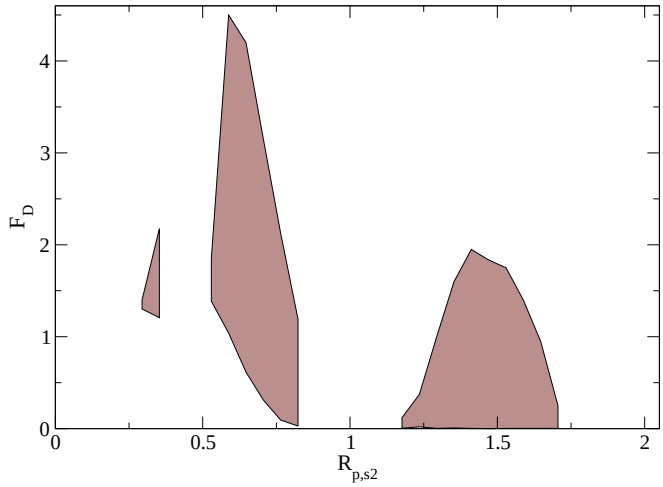

FIG. 24: A plot of F_D vs $R_{p,s2}$ for the system in Fig. 24 indicating the three regions in which negative drag of the particles in s_2 occurs.

E. Five Dynamical Phases

In Fig. 23 we plot the dynamic phase diagram of F_D versus $R_{p,s2} = N_p/N_{s2}$ for a system which exhibits all five phases as well as several regions where a negative drag effect occurs. Here we vary N_p and fix $R_{s2,s1} = 1.133$ and $d/a_{s1} = 0.833$, where a_{s1} is the spacing of the particles in s_1. For this choice of parameters, we observe region V only at $R_{p,s2} = 1.0$, the value shown in Fig. 21. At $R_{p,s2} = 0.882$, which also corresponds to $R_{s1,p} = 1.0$, there is a single transition from region I to region III, indicated by the dashed line. Here the particles in p and s_1 are locked because they are commensurate. The dynamics for $0.6 < R_{p,s2} < 1.75$ is dominated by region IV. For $1.75 \leq R_{p,s2} < 1.95$, a transition from region IV to region II occurs at higher F_D. The location of this transition shifts to higher values of F_D as $R_{p,s2}$ drops below $R_{p,s2} = 1.95$. For $R_{p,s2} \geq 1.95$, the system goes directly into region II for finite F_D. Region II appears for high $R_{p,s2}$ since as N_p increases, the effectiveness of the coupling between the particles in p and the particles in s_1 and s_2 decreases. As a result, even though the particles in s_1 and s_2 are incommensurate, the coupling between the primary and secondary channels eventually becomes so weak that the particles in s_1 and s_2 couple with each other and decouple from the particles in p. At $R_{p,s2} = 0.58825$ there is another peak in the transition out of region I produced by the commensurability condition of $R_{s1,p} = 2/3$ at this filling. For $R_{p,s2} < 0.6$, region I grows in extent and there is a window of region III which separates region I at low drives and region IV at higher drives. For $R_{p,s2} < 0.15$, there is a single transition from region I directly to region IV.

In Fig. 24 we indicate the regions in the F_D versus $R_{p,s2}$ plot where negative drag of the particles in s_2 occurs for the system in Fig. 23, and in Fig. 25 we show

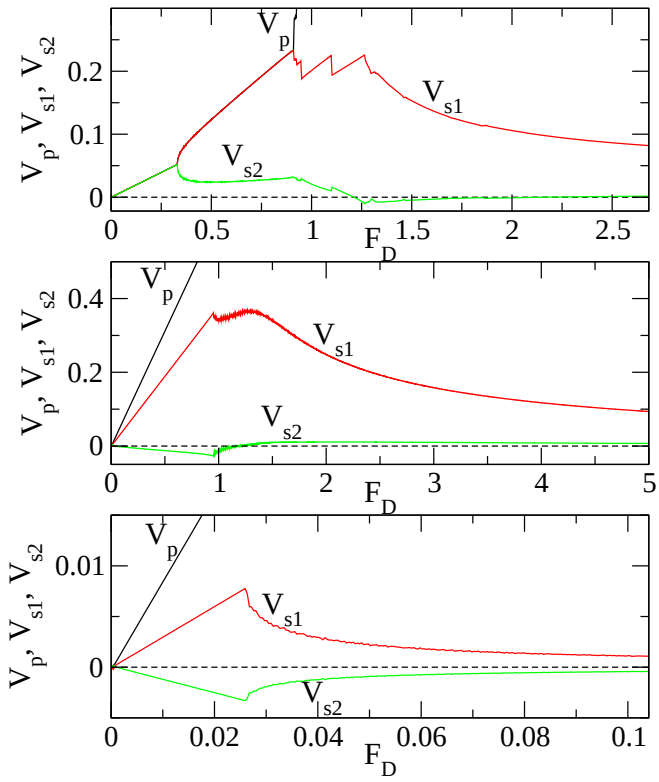

FIG. 25: Representative velocity force curves V_p, V_{s1}, and V_{s2} vs F_D from each of the three regions where negative drive occurs in Fig. 24. (a) $R_{p,s2} = 0.35$. (b) $R_{p,s2} = 0.823$. (c) $R_{p,s2} = 1.53$.

representative velocity force curves for the three different negative drag regions. In Fig. 24 the largest region of negative drag occurs for $0.52 < R_{p,s2} < 0.82$. There is a small negative drag window near $R_{p,s2} = 0.3$. We illustrate a typical velocity force curve from this window in Fig. 25(a) where we plot V_p, V_{s1}, and V_{s2} for $R_{p,s2} = 0.35$. Here the negative drag occurs in region IV. There are also a number of slip events which appear as sharp changes in V_{s1} near $F_D = 1.25$. For higher F_D beyond what is shown in the figure, V_{s2} continues to increase back above zero, passes through a broad peak, and then slowly decreases back toward zero at high F_D. In Fig. 25(b) we plot the velocity force curves at $R_{s2,p} = 0.823$ where the system exhibits only region IV flow. Here the maximum negative value of V_{s2} occurs at $F_D = 0.95$ in the form of a cusp which is accompanied by a cusplike peak in V_{s1}. For $0 < F_D < 0.96$, V_{s1} increases linearly with increasing F_D but the particles in s_1 are not completely locked with the particles in p. This corresponds to region IV^A as was discussed earlier; however, in the phase diagram of Fig. 23 we omit the distinction between regions IV^A and IV^B for clarity. In Fig. 25(c) we plot the velocity force curves at $R_{p,s2} = 1.53$ in the third region of negative drag. Here we find that the magnitude of the maximum negative velocity in V_{s2} is reduced compared to the other

two negative drag regions.

The general features of the phases outlined so far also occur for other parameters of density and filling, indicating that they are robust features of the system. We have not observed negative drag of the particles in s_1 or p.

V. DISCUSSION AND SUMMARY

We investigated a simple system consisting of two or three coupled 1D channels of particles interacting via a repulsive Yukawa potential where only one of the channels is driven. For two channel systems with an equal number of particles in each channel, we find a single transition from a completely locked state to a partially decoupled state where particles in the secondary channel slip with respect to particles in the driven channel. In the decoupled state, the velocity of the particles in the secondary channel gradually decreases with increasing drive while the velocity of the driven particles increases linearly with increasing drive. When the number of particles in the secondary channel is slightly away from commensuration with the number of particles in the primary channels, a two stage decoupling transition occurs where the first decoupling is associated with individual slips of the incommensurations or vacancies in the secondary channel. The velocity of the particles in the secondary channel continues to increase with increasing drive until the second decoupling transition is reached, whereupon all the particles in the secondary channel begin to slip. The driving force at which the transition from the completely locked to the decoupled flow occurs has peaks at integer commensurate ratios of the number of particles in the two channels as well as at certain fractional ratios such as 1/2 or 3/2; however, there are no peaks for low filling ratios since the particles in the driven channel are effectively moving not over a fixed substrate but over a distortable substrate. We also observe a ratchet effect in the two channel system where the particles in the secondary channel can be rectified by an asymmetric ac drive applied to the primary channel. This ratchet effect is similar to the ratchet effect found for coupled binary particle species where only one species is driven.

For three channels we find that a remarkably rich variety of dynamical phases such as coupling and decoupling transitions are possible and produce a variety of commensuration effects as well as pronounced signatures in the velocity force curves. The commensuration effects occur whenever the ratio of the number of particles in at least two of the channels is an integer or rational fraction. We also observe a negative drag effect for the secondary channel which is furthest from the driven channel. Here, the particles in the secondary channel move in the direction opposite to the driving direction of the primary channel. When the negative drag occurs, all three channels have incommensurate fillings. The resulting multiple periodic forces experienced by the particle in the furthest secondary channel create a bi-harmonic ratchet effect of a type that has been observed in systems driven with multiple ac drives.

Our results could be tested for colloidal particles confined to two or three channels where one of the channels is driven by optical means or via microfluidics. Since the motion of physical colloids is never perfectly one-dimensional, some smearing of the effects we observe might occur, but the general features we describe should be observable. A similar experiment could be performed in a dusty plasma system with the dust particles confined in grooves and driven in one dimension with a laser focused in a single plane. Some of the effects we observe could be relevant for certain superconducting vortex systems in which two different types of vortices are coupled and one of the two vortex types is driven with an external current. Additionally, these effects could also be realized using coupled wires in which one-dimensional Wigner crystal states occur. The velocity-force responses that we predict could be a potentially powerful method for determining whether Wigner crystals are actually present in the wires. It would also be interesting to study ratchet effects with asymmetric ac drives for three or more channels. Here, it may be possible to induce dc currents flowing in different directions for different channels. Although the system we consider appears very simple, we have shown that it exhibits a rich variety of behaviors even without substrates or other complications. If a periodic substrate were introduced in one or more of the channels, we expect that an even greater variety of commensuration effects and coupling between excitations in the channels could occur. It would also be interesting to consider cases where the channels are not strictly one-dimensional but have a finite width to allow for transitions to buckled or zig-zag states. Even for the commensurate fillings, such buckling transitions could produce interesting new features in the drag behavior.

This work was carried out under the auspices of the NNSA of the U.S. DoE at LANL under Contract No. DE-AC52-06NA25396.

[1] M. Köppl, P. Henseler, A. Erbe, P. Nielaba, and P. Leiderer, Phys. Rev. Lett. **97**, 208302 (2006); P. Henseler, A. Erbe, M. Köppl, P. Leiderer, and P. Nielaba, Phys. Rev. E **81**, 041402 (2010).

[2] D. McGloin, A.E. Carruthers, K. Dholakia, and E.M. Wright, Phys. Rev. E **69**, 021403 (2004).

[3] R. Haghgooie and P.S. Doyle, Phys. Rev. E **72**, 011405 (2005).

[4] W.P. Ferreira, J.C.N. Carvalho, P.W.S. Oliveira, G.A. Farias, and F.M. Peeters, Phys. Rev. B **77**, 014112 (2008).

[5] W. Yang, K. Nelissen, M. Kong, Z. Zeng, and

F.M. Peeters, Phys. Rev. E **79**, 041406 (2009).
[6] D.V. Tkachenko, V.R. Misko, and F.M. Peeters, Phys. Rev. E **80**, 051401 (2009).
[7] Q.-H. Wei, C. Bechinger, and P. Leiderer, Science **287**, 625 (2000).
[8] C. Lutz, M. Kollmann, and C. Bechinger, Phys. Rev. Lett. **93**, 026001 (2004).
[9] S. Bleil, P. Reimann, and C. Bechinger, Phys. Rev. E **75**, 031117 (2007).
[10] Y. Roichman, D.G. Grier, and G. Zaslavsky, Phys. Rev. E **75**, 020401(R) (2007).
[11] H.J. Schulz, Phys. Rev. Lett. **71**, 1864 (1993).
[12] L.I. Glazman, I.M. Ruzin, and B.I. Shklovskii, Phys. Rev. B **45**, 8454 (1992).
[13] J. Baker and A.G. Rojo, J. Phys.: Condens. Mat. **13**, 5313 (2001).
[14] E.J. Mueller, Phys. Rev. B **72**, 075322 (2005).
[15] V.V. Deshpande and M. Bockrath, Nature Phys. **4**, 314 (2008).
[16] W.K. Hew, K.J. Thomas, M. Pepper, I. Farrer, D. Anderson, G.A.C. Jones, and D.A. Ritchie, Phys. Rev. Lett. **102**, 056804 (2009).
[17] G. Piacente, I.V. Schweigert, J.J. Betouras, and F.M. Peeters, Phys. Rev. B **69**, 045324 (2004); G. Piacente, G.Q. Hai, and F.M. Peeters, Phys. Rev. B **81**, 024108 (2010).
[18] H. Ikegami, H. Akimoto, and K. Kono, Phys. Rev. Lett. **102**, 046807 (2009).
[19] J.S. Meyer and K.A. Matveev, J Phys.: Condens. Mat. **21**, 023203 (2009).
[20] G. Piacente and F.M. Peeters, Phys. Rev. B **72**, 205208 (2005).
[21] B. Liu, K. Avinash, and J. Goree, Phys. Rev. Lett. **91**, 255003 (2003); B. Liu and J. Goree, Phys. Rev. E **71**, 046410 (2005).
[22] G. Coupier, M. Saint Jean, and C. Guthmann, Phys. Rev. E **73**, 031112 (2006); C. Coste, J.-B. Delfau, C. Even, and M. Saint Jean, Phys. Rev. E **81**, 051201 (2010).
[23] R. Besseling, R. Niggebrugge, and P.H. Kes, Phys. Rev. Lett. **82**, 3144 (1999); N. Kokubo, R. Besseling, V.M. Vinokur, and P.H. Kes, Phys. Rev. Lett. **88**, 247004 (2002).
[24] N. Kokubo, T.G. Sorop, R. Besseling, and P.H. Kes, Phys. Rev. B **73**, 224514 (2006)
[25] P. Barrozo, A.A. Moreira, J.A. Aguiar, and J.S. Andrade, Phys. Rev. B **80**, 104513 (2009).
[26] K. Yu, M.B.S. Hesselberth, P.H. Kes, and B.L.T. Plourde, Phys. Rev. B **81**, 184503 (2010).
[27] C.J. Olson Reichhardt and C. Reichhardt, Phys. Rev. B **81**, 224516 (2010).
[28] I. Giaever, Phys. Rev. Lett. **15**, 825 (1965).
[29] J.R. Clem, Phys. Rev. B **9**, 898 (1974).
[30] J.W. Ekin, B. Serin, and J.R. Clem, Phys. Rev. B **9**, 912 (1974)
[31] T. Pe, M. Benkraouda, and J.R. Clem, Phys. Rev. B **56**, 8289 (1997).
[32] M. Yamamoto, M. Stopa, Y. Tokura, Y. Hirayama, and S. Tarucha, Science **313**, 204 (2006); M. Yamamoto, H. Takagi, M. Stopa, and S. Tarucha, AIP Conf. Proc. **893**, 747 (2007).
[33] A review of commensurate-incommensurate transitions appears in P. Bak, Rep. Prog. Phys. **45**, 587 (1982).
[34] S.N. Coppersmith, D.S. Fisher, B.I. Halperin, P.A. Lee, and W.F. Brinkman, Phys. Rev. B **25**, 349 (1982).
[35] M. Baert, V.V. Metlushko, R. Jonckheere, V.V. Moshchalkov, and Y. Bruynseraede, Phys. Rev. Lett. **74**, 3269 (1995); J.I. Martín, M. Vélez, J. Nogués, and I.K. Schuller, Phys. Rev. Lett. **79**, 1929 (1997); S. Avci, Z.L. Xiao, J. Hua, A. Imre, R. Divan, J. Pearson, U. Welp, W.K. Kwok, and G.W. Crabtree, Appl. Phys. Lett. **97**, 042511 (2010).
[36] C. Reichhardt, C.J. Olson, and F. Nori, Phys. Rev. B **57**, 7937 (1998); G.R. Berdiyorov, M.V. Milosević, and F.M. Peeters, Phys. Rev. B **74**, 174512 (2006).
[37] M. Baert, V.V. Metlushko, R. Jonckheere, V.V. Moshchalkov, and Y. Bruynseraede, Europhys. Lett. **29**, 157 (1995); C. Reichhardt and N. Grønbech-Jensen, Phys. Rev. B **63**, 054510 (2001).
[38] A. Chowdhury, B.J. Ackerson, and N.A. Clark, Phys. Rev. Lett. **55**, 833 (1985); C. Bechinger, M. Brunner, and P. Leiderer, Phys. Rev. Lett. **86**, 930 (2001).
[39] C. Reichhardt and C.J. Olson, Phys. Rev. Lett. **88**, 248301 (2002); M. Brunner and C. Bechinger, Phys. Rev. Lett. **88**, 248302 (2002); K. Mangold, P. Leiderer, and C. Bechinger, Phys. Rev. Lett. **90**, 158302 (2003).
[40] C. Reichhardt, C.J. Olson, and F. Nori, Phys. Rev. Lett. **78**, 2648 (1997); J. Gutierrez, A.V. Silhanek, J. Van de Vondel, W. Gillijns, and V.V. Moshchalkov, Phys. Rev. B **80**, 140514(R) (2009); C. Reichhardt and C.J. Olson Reichhardt, Phys. Rev. B **81**, 024510 (2010).
[41] O.M. Braun, A.R. Bishop, and J. Röder, Phys. Rev. Lett. **79**, 3692 (1997); J. Tekić, O.M. Braun, and B. Hu, Phys. Rev. E **71**, 026104 (2005); Y. Yang, W.-S. Duan, J.-M. Chen, L. Yang, J. Tekić, Z.-G. Shao, and C.-L. Wang, Phys. Rev. E **82**, 051119 (2010).
[42] S. Savel'ev and F. Nori, Nature Mater. **1**, 179 (2002).
[43] D. Cole, S. Bending, S. Savel'ev, A. Grigorenko, T. Tamegai, and F. Nori, Nature Mater. **5**, 305 (2006).
[44] M. Tesei, G.K. Perkins, A.D. Caplin, L.F. Cohen, and T. Tamegai, Supercond. Sci. Technol. **21**, 075019 (2008).
[45] M. Das, G. Ananthakrishna, and S. Ramaswamy, Phys. Rev. E **68**, 061402 (2003); R. Messina and H. Löwen, Phys. Rev. E **73**, 011405 (2006).
[46] C. Reichhardt and C.J. Olson Reichhardt, Phys. Rev. E **79**, 061403 (2009).
[47] Z. Jiang, D.A. Dikin, V. Chandrasekhar, V.V. Metlushko, and V.V. Moshchalkov, Appl. Phys. Lett. **84**, 5371 (2004).
[48] A. Libál, C. Reichhardt, and C.J. Olson Reichhardt, Phys. Rev. Lett. **97**, 228302 (2006); A. Libál, C. Reichhardt, and C.J. Olson Reichhardt, Phys. Rev. E **75**, 011403 (2007).
[49] M. Rex and H. Lowen, Eur. Phys. J. E **26**, 143 (2008).
[50] P. Reimann, Phys. Rep. **361**, 57 (2002).
[51] C. Reichhardt, C.J. Olson Reichhardt, and M.B. Hastings, Phys. Lett. A **342**, 162 (2005).
[52] C. Reichhardt, C.J. Olson, and M.B. Hastings, Phys. Rev. Lett. **89**, 024101 (2002); R. Guantes and S. Miret-Artés, Phys. Rev. E **67**, 046212 (2003); C. Reichhardt and C.J. Olson Reichhardt, Phys. Rev. E **68**, 046102 (2003); V. Lebedev and F. Renzoni, Phys. Rev. A **80**, 023422 (2009); D. Speer, R. Eichhorn, and P. Reimann, Phys. Rev. Lett. **102**, 124101 (2009).
[53] A. Libál, C. Reichhardt, B. Jankó, and C.J. Olson Reichhardt, Phys. Rev. Lett. **96**, 188301 (2006).

[54] L. Machura and J. Luczka, Phys. Rev. E **82**, 031133 (2010).